Published in final edited form as:
Soft Matter. 2010 October 21; 6(20): 5143–5156. doi:10.1039/C0SM00642D.

Injectable solid hydrogel: mechanism of shear-thinning and immediate recovery of injectable β-hairpin peptide hydrogels[†,‡]

Congqi Yan[a], **Aysegul Altunbas**[a], **Tuna Yucel**[§,a], **Radhika P. Nagarkar**[¶,b], **Joel P. Schneider**[‖,b], and **Darrin J. Pochan**[a,*]

[a]Department of Materials Science and Engineering and Delaware Biotechnology Institute, University of Delaware, Newark, DE 19716, USA

[b]Department of Chemistry and Biochemistry, University of Delaware, Newark, DE 19716, USA

Abstract

β-Hairpin peptide-based hydrogels are a class of injectable hydrogel solids with significant potential use in injectable therapies. β-hairpin peptide hydrogels can be injected as preformed solids, because the solid gel can shear-thin and consequently flow under a proper shear stress but immediately recover back into a solid on removal of the stress. In this work, hydrogel behavior during and after flow was studied in order to facilitate fundamental understanding of how the gels flow during shear-thinning and how they quickly recover mechanically and morphologically relative to their original, pre-flow properties. While all studied β-hairpin hydrogels shear-thin and recover, the duration of shear and the strain rate affected both the gel stiffness immediately recovered after flow and the ultimate stiffness obtained after complete rehealing of the gel. Results of structural analysis during flow were related to bulk rheological behavior and indicated gel network fracture into large (>200 nm) hydrogel domains during flow. After cessation of flow the large hydrogel domains are immediately percolated which immediately reforms the solid hydrogel. The underlying mechanisms of the gel shear-thinning and healing processes are discussed relative to other shear-responsive networks like colloidal gels and micellar solutions.

Introduction

Researchers are working diligently to develop injectable therapies, such as cell therapy and drug delivery systems, that can be delivered to a targeted *in vivo* site *via* simple syringe or catheter injection, a benign treatment[1–3] relative to traditional surgical implantation.[4–6] Ever increasing efforts have been dedicated specifically to the design and development of hydrogel systems as the delivery vehicles for injectable therapeutics.[1–3,7,8] While the hydrogel scaffolds will have physical and chemical requirements unique to the desired use (*e.g.* a chemotherapeutic drug-eluting hydrogel for glioblastoma treatment in the brain would have different biological and physical requirements than a delivery scaffold for stem cell delivery to the dynamic environment of infarcted myocardial tissue), all designed hydrogels must generally be biocompatible; the scaffolds should cause acceptable, limited

[†]This paper is part of a joint *Soft Matter and Journal of Materials Chemistry* themed issue on Tissue Engineering. Guest editors: Molly Stevens and Ali Khademhosseini.

[‡]Electronic supplementary information (ESI) available: Additional rheology results (gelation kinetics and gel restoration kinetics) and small-angle neutron scattering measurements. See DOI: 10.1039/c0sm00642d

pochan@udel.edu; Fax: +302-831-4545; Tel: +302-831-3569.
[§]Present address: Department of Biomedical Engineering, Tufts University, Medford, MA 02155, USA
[¶]Present address: Glaxosmithkline Biopharm R&D, 709 Swedeland Road, King of Prussia, PA 19406, USA
[‖]Present address: Chemical Biology Laboratory, Center for Cancer Research, National Cancer Institute, Frederick, MD 21702, USA

levels of inflammation and immunogenic response in the host. It may also be advantageous for some hydrogel systems to be biodegradable and/or resorbable by the host. Particularly crucial for potential injectable drug delivery and tissue regeneration therapies is the ability of an injected system to stay localized at the region of injection; the material must adequately resist biological flows and forces *in vivo* that work to move or dilute the injected system so as to provide the therapy to the desired, specific area.[2,9,10] Mechanical properties are, therefore, particularly important in the design of injectable scaffolds since the ability of the injected system to remain localized as a well-defined material is directly related to stiffness and network structure of the scaffold.[9,10] In addition, hydrogel mechanical properties are key biological criteria to address[7,9,10] since the transplanted gel matrix stiffness can directly impact local cell adhesion and morphology, viability and gene expression.[11–18]

The most prevalent strategy for injectable hydrogel scaffolds is to design a free flowing solution that easily can be injected as a low viscosity liquid and subsequently form a solid hydrogel *in vivo*. It should be emphasized that before injection these materials are *easily flowing solutions ex vivo*. Once these solutions reach *in vivo*, a sol–gel transition can be triggered by physiological cues such as enzymes,[19–23] salt[24–30] or a temperature change.[31–39] Additionally, the gel network can be formed *via* photo-initiated polymerization or cross-linking.[40–45] Since these *in vivo*-forming gel systems are injected as free flowing solutions, they can easily fill well-defined defects and cavities of arbitrary shape.[1] However, the free flowing property that allows easy injection also can lead to unwanted leakage of these gelprecursor solutions into neighboring tissue or the blood stream unless the filled defect has a natural boundary to contain the injected liquid.[46] Leakage and flow can be minimized with higher viscosity precursors[45] or fast *in situ* gelation kinetics. Once injected, it is difficult to unambiguously characterize the *in vivo* material properties of hydrogels formed from cross-linkable liquids. This is because after the precursor solutions experience flow into the *in vivo* environment[47] the injected solutions can be diluted by local bodily fluids and/or affected by the local environment prior to, or during, crosslinking.

An alternate, more recent strategy for injectable hydrogel therapies is the development of new, solid hydrogel scaffolds that can shear-thin and consequently flow under a proper shear stress but recover back into solids upon removal of the stress. To reemphasize, this strategy involves the *ex vivo* formation of a desired *solid gel* with desired mechanical, morphological, and biological properties. The shear-thinning property enables the preformed, solid gel to be injected as a low viscosity, flowing material. Once injection shear is removed, restoration of gel rigidity allows the hydrogel, together with the desired payloads that were encapsulated during the original hydrogelation, to remain localized at the point of injection.[9,10] The phenomenon of gel networks shear-thinning, flowing and reforming is something that has been studied significantly in colloidal gels. Colloidal gels, gel networks comprised of percolated, colloidal particles,[48,49] can also undergo a reversible gel–sol transition upon application of shear and, thereby, display shear-thinning rheological behavior[50–52] and interesting aging behavior.[53,54] A large area of current research is the investigation of colloidal gel network microstructure at rest and under flow.[50–52,55–61] Recent work also attempts to relate results of colloidal gel structural analysis to bulk rheological behavior in order to understand how networks are disassembled and reformed.[50,51,56] While colloidal gel materials are quite different physically to the gel networks to be discussed herein (*e.g.* colloidal microscale particles vs. peptidic nanofibers), there are many similarities between the yielding, flow and network reformation mechanisms.[50–52,55–62] We will invoke colloidal network mechanisms of network break-up, flow and network reformation (or lack thereof) when we discuss these phenomena in our peptide hydrogel networks later in the paper.

Over the past decade, Pochan and Schneider and coworkers have developed a class of self-assembling β-hairpin peptides[9,63–69] to create physical hydrogels as injectable therapeutic delivery vehicles.[9,70] Beginning in 2002, shear-thinning and self-healing behavior was first observed from these peptide hydrogels when assembled at basic pH.[63] After experiencing oscillatory 1000% strain in a parallel plate rheometer, the shear-thinned gel material immediately recovered into a solid gel with the original gel rigidity rapidly restoring over time. Subsequently in 2004, similar shear-reversibility was reported from β-hairpin hydrogels formed under physiological conditions.[71] Furthermore in 2007, hydrogels formed in syringes were found to be capable of being shear-thin delivered to a target position with high precision where, after injection, these materials immediately formed solids and remained localized.[9] Concurrently, these hydrogels were demonstrated to display fundamental properties critical for use as biomaterials such as cytocompatibilty towards several model cell lines,[9,72,73] inability to activate macrophages in an *in vitro* model,[74] and even an innate antimicrobial activity.[67,75] The unique physical gelation and shear-thinning/rehealing behavior, coupled with preliminary, benign biological properties, suggest that these hydrogels are excellent candidates for injectable hydrogel scaffolds that can be injected as preformed solids.

The first peptide studied, MAX1 (VKVKVKVK–V^{D}PPT-KVKVKVKV-NH_2), was comprised of two β strands with alternating hydrophobic valine (V) and hydrophilic lysine (K) residues covalently bonded to a central tetra-peptide turn sequence (V^{D}PPT).[63] When dissolved in neutral pH solution with low ionic strength, MAX1 peptide remains unfolded and random coil-like because of repulsion between positively charged lysine side groups. The electrostatic repulsion can be mitigated by deprotonation of the lysines at basic pH,[63] a rise in temperature to induce hydrophobic collapse,[64] or the addition of salt solution or salt in a cell culture medium to screen electrostatic interactions.[71] In response, the peptides undergo a conformational change and fold into β-hairpins causing consequent self-assembly into a rigid, fibrillar hydrogel stabilized by physical crosslinks[71,76,77] that allow them to shear-thin. In order to tailor properties for a specific biomedical use (*e.g.* controlled release of desired therapeutics), gel stiffness and porosity can be changed by manipulation of peptide assembly kinetics through alteration of peptide concentration, solution ionic strength, temperature and/or by modification of the peptide sequence.[9,70,76,78] For example, a more recent peptide, MAX8 (VKVKVKVK–V^{D}PPT-KVEVKVKV-NH_2), was designed to have the same primary structure as MAX1 except that the lysine residue at position 15 was replaced with a glutamic acid (E) residue. Due to a change in overall peptide charge, this sequence modification enabled gelation kinetics under physiological condition faster than the original MAX1 sequence, important for desired, homogeneous, three-dimensional cell encapsulation for injectable delivery of cells.[9] The shear-thinning property allowed the MAX8 gel-cell construct to be delivered *via* a syringe needle while the self-healing behavior enabled the construct to remain localized after syringe injection. It was also observed that shear-thin delivery had little or no effect on encapsulated cell viability and three dimensional cell distribution.[9] To re-emphasize, these results reflect the potential of this strategy to form final gel material *in vivo* that will retain the same properties as the hydrogel exhibited *ex vivo*. Therefore, one can establish direct bioproperty/gel structure relationships *in vivo* and *in vitro*.

From the beginning of the β-hairpin hydrogel studies, rheological property has been highlighted as an important material characteristic to address for injectable hydrogels.[9,63–82] This rheological perspective has also been appreciated by other groups that have more recently used rheology to observe the viscoelastic behavior in different biomaterial hydrogel systems.[24,25,28,29,36,83–91] Most of these studies included oscillatory rheological measurements in order to determine whether molecule chemistry, sample conditions or environmental factors affected gelation kinetics or gel rigidity. Some recent studies have

also begun to probe shear-thinning behavior in different biomaterial hydrogel systems with oscillatory shear rheology.[28,92] As stated earlier, we have identified that solid β-hairpin peptide hydrogels shear-thin and flow under mechanical shear and immediately recover back into solid gels upon cessation of shear. However, to date, β-hairpin peptide hydrogel gel shear-thinning and healing behavior was only examined in limited rheological conditions with the underlying mechanisms unexplored. In this work, we investigate hydrogel structure and mechanical behavior during and after flow in order to understand how these gel materials flow and how they recover relative to their original, pre-flow properties. These measurements essentially relate gel network structure during shear to the bulk rheological behavior, which unveils the underlying mechanisms of shear-thinning and recovery processes. The results help explain the ability of the (β-hairpin peptide hydrogels to immediately recover into solids after injection flow as well as how encapsulated payloads are affected by flow, a critical consideration for biomedical applications.

Experimental session

Hydrogel preparation

MAX1 (VKVKVKVK–V^{D}PPT-KVKVKVKV-NH_2) and MAX8 (VKVKVKVK–V^{D}PPT-KVEVKVKV-NH_2) peptides were synthesized, respectively, on Rink amide resins with an automated SONOTA peptide synthesizer employing standard Fmoc-protocol and HCTU activation. Detailed description of peptide synthesis and purification is available in a previously published protocol.[63,93] To prepare a MAX1 hydrogel sample, pure MAX1 peptide was first dissolved in chilled DI water to produce a peptide stock solution. Then an equal volume of chilled 100 mM bis-tris-propane (BTP) buffer solution (pH 7.4) was added to adjust peptide concentration, pH and ionic strength to desired final conditions (1 or 2 wt %; pH 7.4; 150 or 400 mM NaCl). Similarly, 0.5 wt% MAX8 hydrogel was prepared by dissolving 2.5 mg pure MAX8 peptide in 250 μL 25 mM HEPES buffer (pH 7.4) and by subsequent addition of 250 μL 1X DMEM with 25 mM HEPES (pH 7.4). While MAX8 gels were studied under physiological mimicking conditions, MAX1 was studied under physiological as well as high salt conditions. These high salt conditions allow the control of MAX1 hydrogel physical properties in order to observe their affects on the shear thinning and rehealing behavior.

Rheology

Oscillatory rheology experiments were performed on an AR-2000 rheometer (TA Instruments) using a 40 mm-diameter acrylic, cross-hatched parallel plate geometry tool. Each buffered peptide solution was prepared in ice-chilled solutions to prevent thermal gelation. To study gel restoration kinetics after shear disruption, hydrogels were formed either directly on the rheometer or within a syringe. In the former situation, the buffered peptide solution was quickly transferred to the rheometer bottom plate that was pre-equilibrated at 5 °C. The parallel plate geometry tool was then lowered to a desired gap height, 0.2 mm for MAX1 and 0.25 mm for MAX8, in order to delay edge effects.[94] A NIST traceable standard S3 mineral oil (Cannon Instruments, $\eta \approx 3$ mPa s at 22 °C) was applied around the plate geometry tool to prevent sample drying. Then the temperature was ramped linearly and quickly to either 20 °C for MAX1 or 37 °C for MAX8 to initiate gelation. First, a dynamic time sweep was performed to measure the time-dependent evolution of storage (G') and loss (G'') moduli during gelation at a frequency of 6 rad s^{-1} and 0.2% strain until the gel equilibrated. Then steady shear flow was applied to disrupt the gel *in situ* with the shear treatment (shear duration and shear rate) varied from sample to sample. Once the shear flow was ceased, restoration of gel rigidity was immediately monitored over time in a subsequent dynamic time sweep (6 rad s^{-1} and 0.2% strain). In addition, dynamic frequency sweeps (0.1–100 rad s^{-1}, 0.2% strain) and dynamic strain sweep (6 rad s^{-1} and 0.1–1000%

strain) were also performed on equilibrated gels formed directly on the rheometer, the results of which are provided in the ESI.‡ For injection studies of hydrogel formed within a syringe, the buffered peptide solution was equilibrated in the syringe at the desired temperature for two hours to ensure stabilization of the expected solid hydrogel. Then the hydrogel was injected through a 26 gauge needle onto the bottom plate of the rheometer that was pre-equilibrated at 20 °C for MAX1 gel or 37 °C for MAX8 gel. After quickly lowering the upper tool to the desired gap height (0.2 mm for MAX1 and 0.25 mm for MAX8 gels) and applying the S3 mineral oil to prevent sample evaporation, a dynamic time sweep (6 rad s^{-1} and 0.2% strain) was immediately started to measure restoration of gel stiffness over time.

Rheo-small-angle neutron scattering (SANS)

Rheo-SANS experiments were conducted on a 30 m SANS instrument, NG7, equipped with a Paar Physica UDS 200 rheometer at the National Center for Neutron Research at the National Institute of Standards and Technology.[95] The instrumental set-up is illustrated in Fig. 1. The neutrons were monochromated to a wavelength of 6 Å with a wavelength spread $\Delta\lambda/\lambda = 0.12$. Scattering patterns of samples during shear flow were obtained at two sample-to-detector distances (1.7 m and 15.3 m) in the radial direction (on-axis),[96,97] covering a scattering vector range of $0.003\ Å^{-1} < q < 0.3\ Å^{-1}$ where $q = (4\pi/\lambda)\sin(\theta/2)$ and θ is the scattering angle. This q range enables observation of gel structure at a length scale between 2 nm and 200 nm in real space. Pure MAX1 and MAX8 peptides were dissolved in D_2O and then lyophilized in order to ensure all the exchangeable peptide protons were exchanged with deuterons. Buffered MAX1 and MAX8 peptide solutions were prepared as described earlier except that DI water previously used to prepare peptide stock solutions and buffers was replaced by D_2O to ensure sufficient scattering contrast. After mixing, each buffered peptide solution was quickly transferred to the quartz Couette shear cell (49 mm inner-diameter, 0.5 mm gap) that was pre-equilibrated at 5 °C. Then the temperature was ramped linearly and quickly to either 20 °C for MAX1 or 37 °C for MAX8 to initiate gelation. After three hours of gelation, the scattering measurement was first conducted on the equilibrated hydrogel at rest. Then the gel was subject to a steady shear flow (10, 100 or 1000 s^{-1}), and corresponding scattering data was collected when the shear viscosity was stable over time. Resulting SANS data were corrected for background electronic noise, detector inhomogeneity, and empty cell scattering according to published protocol.[98] Two different q regimes were covered in two separate scattering experiments with $0.003\ Å^{-1} < q < 0.01\ Å^{-1}$ results shown in Fig. SI-11 and SI-12 (ESI‡) and $0.01\ Å^{-1} < q < 0.3\ Å^{-1}$ results shown in Fig. 11 and 12.

Small-angle X-ray scattering (SAXS)

SAXS experiments were performed at BioCAT beamline, Advanced Photon Source (APS), Argonne National Laboratory (ANL). The instrumental sketch is illustrated in Fig. 2. The flow cell is a cylindrical quartz capillary (1.5 mm inner-diameter) placed vertically and connected to a programmable dual Hamilton syringe pump which drives the sample up and down inside the capillary. The X-ray beam was aimed perpendicular through the capillary cross-section. The wavelength of the synchrotron source was monochromated to 1.033 Å. Scattering patterns of samples during capillary flow were obtained at one sample-to-detector distance of 1.54 m that covered a scattering vector range of $0.012\ Å^{-1} < q < 0.6\ Å^{-1}$. Buffered MAX8 peptide solutions were prepared as described earlier and quickly drawn into the flow cell pre-equilibrated at 37 °C. After two hours of equilibration, SAXS was first performed on the quiescent gel. Then the syringe pump was programmed to make the gel

‡Electronic supplementary information (ESI) available: Additional rheology results (gelation kinetics and gel restoration kinetics) and small-angle neutron scattering measurements. See DOI: 10.1039/c0sm00642d

flow at a constant rate, 10 μL min^{-1}, and a scattering measurement was simultaneously performed on the gel during capillary flow. The shear rate at the capillary wall can be calculated from the equation: $\dot{\gamma}_w = \frac{4Q}{\pi r^3}$, in which Q is volumetric flow rate, r is inner radius of the capillary,[99] where we assumed MAX8 gels behave like Newtonian fluid in laminar flow with no slip at the boundary of capillary. This assumption is reasonable since the shear viscosity of MAX8 gel at 1000/s was measured to be a constant value very close to that of pure water.

Therefore, the shear rate at capillary wall is ~1800 s^{-1} for flow rate of 10 μL min^{-1}. Resulting 2D SAXS data were corrected for background capillary and solvent scattering by using the software Fit2D, available at website of European Synchrotron Radiation Facility (ESRF),[100] and radial scattering intensity was obtained from 2D scattering pattern *via* the MATLAB-based software SAXSGUI (Rigaku, Inc).

Cell culture conditions, cell encapsulation and confocal microscopy

MG63 cells, a progenitor osteoblast cell line from rat osteosarcoma, were cultured in DMEM cell culture media supplemented with 10% fetal bovine serum and 50 μl mL^{-1} Penicilin-Streptomycin. For cell encapsulation experiments the cells were detached from tissue culture flasks with Trypsin-EDTA, counted and resuspended in DMEM with 25 mM HEPES at a concentration of 5×10^6 cells mL^{-1}. An equal volume of this solution was added on top of a peptide solution prepared by dissolving MAX8 in DI water buffered to pH 7.4 with 25 mM HEPES. The cell/gel construct was immediately loaded into a syringe through an 18½ gauge needle. The syringe was placed into the humidified incubator maintained at 37 °C and 5% CO_2 to allow the system to undergo hydrogelation for 5 min. After 5 min, the gel with encapsulated cells inside the syringe was shear-thin delivered onto an 8-well borosilicate confocal chamber (~100 μL gel per well). The cell/gel constructs were overlaid with 300 μL of complete cell culture medium. After 3 h the cell culture medium was removed and overlaid with complete cell culture medium containing 2 mM of calcein acetoxymethylester (calcein AM, cytoplasmic dye) and 4 mM of propidium iodide (PI, nuclear stain) to assess cell viability. The cell/gel constructs were observed with confocal microscopy (LSCM, Zeiss LSM 510 NLO).

Results and discussion

Gel behavior after flow

To elucidate mechanisms of gel recovery after shear-thinning, it is essential to investigate how the hydrogels recover relative to their original, pre-shear rigidity. Previously, it was observed that both MAX1 and MAX8 gels quickly restored their stiffness as a function of time after being deformed by 1000% oscillatory shear strain.[9,63,71] In this work, different shear conditions, rheometer-induced shear flow and syringe injection shear, were adopted to disrupt the gels and, once shear treatment was removed, the restoration of gel stiffness was immediately monitored with an oscillatory measurement over time. For the situation of the rheometer-induced shear treatment, hydrogelation of buffered peptide solutions was initiated *in situ* on the rheometer, and the storage modulus (G′) and loss modulus (G″) were observed as a function of time until they equilibrated (see the ESI‡). The average storage modulus of 2 wt% MAX1 (pH 7.4, 50 mM BTP, 400 mM NaCl) and 0.5 wt% MAX8 (pH 7.4, 25 mM HEPES, DMEM cell culture medium) gels were 2900 ± 200 Pa (as a representative in Fig. SI-1‡) and 400 ± 50 Pa (as a representative in Fig. SI-2‡), respectively, based on 30 samples of each peptide. Hence, equilibrated gels of the same peptide origin were of uniform mechanical stiffness prior to shear treatment. A constant shear rate was then applied to disrupt the stable, solid gel to a low-viscosity, flowing material. Upon cessation of steady

flow shear, restoration of G′ and G″, representative of gel recovery, was immediately monitored over time.

To study effects of shear rate and shear duration on gel restoration kinetics, shear treatment applied on each gel sample was varied either by shear duration while holding shear rate constant, or by shear rate while holding shear duration constant. In the first scheme, three MAX1 gels formed on the rheometer were individually subject to a constant shear rate of 1000 s^{-1} that lasted for 5, 40 or 120 s. Fig. 3 exhibits corresponding post-shear restoration of G′ over time. Immediately after cessation of shear, all three MAX1 samples exhibited solid gel responses with appreciable G′ values close to 100 Pa or greater and significantly higher than G″ (Fig. SI-3‡) in all cases with this difference between G′ and G″ increasing with time and further network healing. The inset of Fig. 3 indicates that the initial G′ measured right after shear flow was stopped is dependent on shear duration applied. For the three MAX1 hydrogel samples sheared for 5, 40, 120 s at 1000 s^{-1}, the corresponding value of immediately restored G′ was 440 Pa, 180 Pa, 86 Pa, respectively. Also, two hours later, G ′ of recovering MAX1 gels was 95%, 76%, 65% that of the original equilibrated modulus prior to shear flow, respectively (2900 Pa, Fig. SI-1‡). These results altogether indicate that restoration of gel solid-like properties is immediate albeit with lower initial G′ values relative to pre-shear values. The long time recovery of the gel stiffness is less complete after a longer length of shear duration, but short shear treatments, similar to what would be expected during an injection, leave the final material after flow almost unchanged from the original, pre-flow material rheological properties.

In the second scheme, MAX1 gels formed on the rheometer were individually subject to a constant shear rate of 10 s^{-1}, 100 s^{-1}, 1000 s^{-1} that lasted for 40 s. Fig. 4 exhibits corresponding post-shear restoration of G′ over time. Right after cessation of shear, all three MAX1 samples immediately exhibited solid gel network behavior (initial G′ > G″, as shown in Fig. SI-4,‡ with all G′ values ≥ 180 Pa). The inset of Fig. 4 indicates that the initial G′ assessed immediately after shear flow was stopped is dependent on the shear rate applied. For the three MAX1 hydrogel samples sheared at 10 s^{-1}, 100 s^{-1}, and 1000 s^{-1} the corresponding value of initial G′ is 1223 Pa, 430 Pa, and 180 Pa, respectively. After two hours of restoration, G′ of recovering MAX1 gels is 82%, 78%, 76% that of original equilibrated modulus (2900 Pa, Fig. SI-1‡). These results indicate that restoration of gel rigidity will start from an initial G′ that is lower than the original, preshear G′ value, but yet clearly indicative of solid-like gel behavior. In addition, the ultimate gel storage modulus will be lower than the preshear value, and the magnitude of ultimate modulus is dependent on the shear rate during the gel flow.

For the situation of shear induced by syringe injection, hydrogelation of buffered 2 wt% MAX1 peptide solution was initiated in a 5mL syringe and allowed to equilibrate at 20 °C overnight. After the MAX1 hydrogel was injected through a 26 gauge needle onto the rheometer, measurement of G′ (Fig. 5) as a function of time was performed immediately. On initiation of the oscillatory measurement, the MAX1 sample had recovered into a solid gel (Fig. SI-5‡) with G′ further evolving with time (Fig. 5), which is similar to self-restoring behavior of MAX1 gels in the situation of rheometer-induced shear treatment. The fact that MAX1 hydrogels displayed consistent recovery properties despite difference of shear conditions (rheometer *vs.* syringe injection) clarifies that the observed shear-thinning and recovery behavior after flow is representative of authentic bulk gel properties rather than, for example, a simple result of rheometer artifact such as wall slip during large strain treatments on the rheometer. This will be addressed further later in the discussion.

Self-healing behavior of MAX8 gels was also investigated under the same shear conditions. Although 0.5 wt% MAX8 hydrogels (average G′ of 400 Pa, Fig. SI-2‡) are less stiff than 2

wt% MAX1 hydrogels (average G′ of 2900 Pa, Fig. SI-1‡), all the samples studied were capable of recovering into solid gel networks immediately after shear treatment was removed. Like MAX1 gels, the resulting recovery of MAX8 hydrogels is dependent on shear duration applied (Fig. 6). The inset of Fig. 6 indicates that for the three MAX8 hydrogel samples sheared for 5, 40, 120 s, the corresponding value of initial G′ is 21 Pa, 10 Pa, 4 Pa, respectively. Also, two hours later, G′ of recovering MAX8 gels is 89%, 80%, 77% that of original equilibrated modulus prior to shear flow, respectively (400 Pa, Fig. SI-2‡). Recovery of MAX8 hydrogels also depends on shear rate applied (Fig. 7). The inset of Fig. 7 indicates that for the three MAX8 hydrogel samples sheared at 10 s^{-1}, 100 s^{-1}, and 1000 s^{-1} the corresponding value of initial G′ is 199 Pa, 72 Pa, and 10 Pa, respectively. After two hours of restoration, G′ of recovering MAX8 gels is 98%, 86%, 80% that of original equilibrated modulus. These results demonstrate that, like MAX1 gels, MAX8 gels also exhibit immediate post-shear G′ lower than the preshear G′ value but they immediately attain solid gel behavior after shear (Fig. SI-6 and SI-7‡). The stiffness recovery of MAX8 gels after shear is similarly incomplete under longer shear duration or higher shear rate. Importantly, MAX8 hydrogels displayed consistent time-dependent hydrogel recovery from shear conditions induced both by the rheometer and syringe injection (Fig. 8). Again, it is reasonable to believe that the flow and recovery gel behaviors observed in the two different geometries represent authentic bulk gel properties.

In addition to impact of shear treatment on gel recovery behavior, we also studied the role that pre-shear gel stiffness plays in gel restoration by varying peptide concentration and ionic strength. Previously, it was observed that MAX1 hydrogel self-assembled at higher peptide concentrations had higher equilibrated moduli.[76] Also, it was demonstrated that higher ionic strength gave rise to faster self-assembly kinetics and, therefore, a stiffer hydrogel.[71] To vary peptide concentration, two MAX1 hydrogels of 1 and 2 wt% peptide (all with pH 7.4, 50 mM BTP, 400 mM NaCl) were prepared directly on the rheometer resulting in hydrogels with G′ = 1227 and 2900 Pa, respectively. To vary ionic strength, another two 2 wt% MAX1 gel samples were prepared directly on the rheometer with ionic strength of 150 mM and 400 mM of added NaCl (pH 7.4, 50 mM BTP) resulting in hydrogels with G′ = 579 and 2900 Pa, respectively. After initial gel formation and equilibration, all four of these samples were subjected to a constant shear rate of 1000 s^{-1} for 40 s. Upon cessation of shear flow, every sample immediately recovered into a solid hydrogel network as indicated by appreciable G′ values well above corresponding G″ values (Fig. SI-9 and SI-10‡). For the 1 wt% and 2 wt% MAX1 hydrogel samples, the corresponding value of immediate G′ recovered post-shear was 139 Pa and 180 Pa, 11% and 6% that of original equilibrated modulus, respectively (Fig. 9b). After two hours of restoration, G′ of the recovering MAX1 gels was 79% and 76% (Fig. 9a) that of original equilibrated modulus, respectively. For the two MAX1 hydrogel samples with 150 mM and 400 mM NaCl, the corresponding value of G′ immediately post-shear was 47 Pa and 180 Pa, 8% and 6% that of original equilibrated modulus respectively (Fig. 10b). After two hours of restoration, G′ of the recovering MAX1 gels was 88% and 76% (Fig. 10a) that of the original, equilibrated modulus prior to shear flow, respectively. These results demonstrate that for stiffer hydrogels due to higher peptide concentration (Fig. 9) or higher ionic strength (Fig. 10), restoration of gel rigidity started with higher G′ measured right after shear flow with higher, final recovered moduli than gels that were initially less stiff due to lower peptide concentration or lower ionic strength. However, in all cases after shear, the hydrogels recovered approximately the same percentage of stiffness relative to their original, preshear values after two hours of recovery clearly indicative of similar shear-thinning and recovery mechanisms for the gels with different stiffness. This will be discussed further later in the paper.

Dynamic network morphology during flow

Hydrogel structure during steady shear flow was investigated by SANS on hydrogels of MAX1 and MAX8 formed individually in a quartz Couette shear cell. The neutron beam was directed radially towards the Couette cell. The key observation to make is to check whether there is any anisotropy displayed in the resulting 2D scattering patterns. If, for example, the gel network is broken into individual fibrils under shear flow, these fibrils will align along the shear direction resulting in 2D patterns with highly anisotropic features concentrating most scattering intensity perpendicular to the aligned fibril axes.

Radial 2D scattering patterns were collected for MAX1 (Fig. 11 and Fig. SI-11[‡]) and MAX8 (Fig. 12 and Fig. SI-12[‡]) hydrogels at rest and then under steady shear flow within the scattering vector range of 0.003 $Å^{-1} < q < 0.3$ $Å^{-1}$. This q range enables observation of hydrogel structure with length scale between 2 nm and 200 nm in real space. To summarize the SANS results, essentially no anisotropy was observed in any observed scattering patterns. The lack of anisotropy indicates that there is little or no hydrogel fibril nanostructure alignment during steady shear flow. The degree of fibril alignment can be quantified by Herman's orientation function,[101] f, which takes the form $f=\frac{3<\cos^2\phi> - 1}{2}$, in which $<\cos^2\phi>=\frac{\int_0^{\frac{\pi}{2}} I(\phi)\cos^2\phi \sin\phi \, d\phi}{\int_0^{\frac{\pi}{2}} I(\phi) \sin\phi \, d\phi}$.

For each hydrogel sample studied, the annular averaged scattering intensity $I(\phi)$ was obtained from resulting 2D SANS patterns (Fig. 11 and 12) at $q = 0.03$ $Å^{-1}$ as a function of the azimuthal angle, ϕ, with the corresponding values of the orientation function listed in Table 1. At all shear rates investigated, values of the orientation function are within the narrow range from 0 to −0.1. By definition, the orientation function equals 1 for complete alignment of the fiber axes parallel to the direction of interest (*i.e.* flow direction), −0.5 for complete alignment of fiber axis normal to that direction, and 0 for randomly oriented fibers.[101] The orientation results clearly show that fibrils in gel samples under shear flow are essentially randomly oriented, just as in the case of static gels. For comparison's sake, a good example of significant shear alignment during flow is acicular precipitated calcium carbonate particles suspended in poly-(ethylene glycol). These suspensions were observed to display a significant degree of alignment in the flow direction when subjected to the same shear field as used on the β-hairpin peptide hydrogels.[102] Azimuthally integrated, one-dimensional neutron scattering curves of the two-dimensional data, corresponding to hydrogels under various shear rates, overlap well with each other and clearly indicate the identical nanofibrillar structure underlying all of the β–hairpin hydrogels studied here (Fig. SI-13, 14, and 15[‡]). The 1D scattering curves were fit with the summed model, a linear combination of the cylinder form factor, used to describe local structure below ~ 50 nm as determined by the q ranges used for the fit, and the power-law model to describe higher-order network structure at larger length scales greater than ~ 50 nm. The cylinder form factor model describes scattering from a cylindrical solid with radius r and length L, which is defined as

$$P(q)=\frac{\text{scale}}{V_{\text{cyl}}}\int_0^{\pi/2} f^2(q,\alpha)\sin\alpha \, d\alpha$$

and

$$f(q,\alpha)=2(\rho_{cyl}-\rho_{solv})V_{cyl}j_0(qH\cos\alpha)\frac{J_1(qr\sin\alpha)}{(qr\sin\alpha)}$$

in which the volume of cylinder, $V_{cyl} = \pi r^2 L$, $j_0(x) = sin(x)/x$, $L = 2H$, ρ_{cyl} and ρ_{solv} are scattering length densities of cylinder and solvent respectively, α is the angle between the cylinder axis and the scattering vector, q.[98] The power law model takes the form of

$$I(q)=I_0q^{-m}.$$[98]

Therefore, the summed model has the function of $I_{sum} = k_1P(q) + K_2I(q)$ + incoherent background, in which k_1, k_2 are arbitrary constants.

The summed model fit the intensity curves well, and the fitting results are listed in Table 2. For both MAX1 and MAX8 hydrogels studied, fitting results demonstrate that the fibril radius is ~16 ± 2 Å and agrees well with previous scattering and transmission electron microscopy observations.[63,71,72,76–78] These results indicate that the local fibril structure that constitutes the gel network remains cylindrical fibrils with homogeneous diameter despite shear flow.

In order to observe hydrogel structural changes in a geometry similar to actual potential therapeutic uses involving syringe or catheter injection, network morphology at length scales < 50 nm was also probed by SAXS when MAX8 hydrogel flowed through a quartz capillary. As illustrated in Fig. 13, 2D scattering patterns of MAX8 hydrogel at rest and during capillary flow (flow rate = 10 μL min^{-1}, wall shear rate ~1800 s^{-1}, total q range of 0.012 $Å^{-1} < q < 0.6$ $Å^{-1}$) are isotropic. For both conditions, the value of Herman's orientation function at $q = 0.03$ $Å^{-1}$ is −0.08 and −0.105, indicative of minimal fibril alignment during capillary flow. A good contrast in the lack of alignment can be seen in the case of β-lactoglobulin fibers which were found to be strongly aligned under capillary flow *via* small-angle X-ray scattering.[103]

Mechanisms of shear-thinning and self-healing processes

To summarize the experimental results presented earlier, we have studied β-hairpin peptide hydrogel structure and rheological behavior during and after flow. All studied β-hairpin hydrogels shear-thin and flow as a low viscosity material. In shear recovery experiments, all hydrogels immediately recovered into solids after shear treatment regardless of different shear conditions and attained different immediate stiffness after cessation of shear depending on the specific shear rate and duration. Rheology results also indicated that ultimate restoration of gel rigidity was less complete and/or slower in gels that experienced longer shear duration or higher shear rate during gel flow. In rheo-SANS scattering measurements, no anisotropy was displayed in gel network structure from local fibril length scales of several nanometres up to 200 nm at all shear rates studied. In capillary SAXS, no anisotropy was displayed in gel network structure from local fibril length scales of several nanometres up to 50 nm. These scattering observations exclude the possibility of fibril alignment along the flow direction. In addition, one-dimensional neutron intensity curves at all shear rates investigated overlap well with each other and lead to uniform values of fibril diameter *via* fitting. These analyses indicate that the local fibril structure that constitutes the gel network remains cylindrical fibrils with homogeneous diameter despite shear flow.

By relating bulk gel mechanical behavior to structural characterization of dynamic network morphology, a model is proposed (Fig. 14) in order to explain how β-hairpin hydrogel shear-

thin flows and immediately recovers into a stiff network. In fact, the data reveal that the hydrogel network fractures during shear-thinning allowing for flow. The fractured domains provide for subsequent, immediate recovery after flow and continued network self-healing processes over time. Fig. 14 illustrates various stages of gel network structure before, during and after flow. Initially, the equilibrated hydrogel has a fibrillar network structure stabilized by physical crosslinks of fibrillar branching and fibrillar entanglements.[71,77] The application of shear flow fractures the physical, fibrillar network into domains that allow gel flow into a capillary or syringe and subsequent flow along the capillary. The fractured domains must be greater in size than ~200 nm, the largest length scale probed during the scattering experiments in which minimal morphology change or alignment was observed in a flowing gel relative to a pre-sheared, static gel. On removal of the shear stress and consequent flow, the gel domains are immediately percolated and thus form a macroscopic network spanning the entire gel giving a solid-like mechanical response ($G' > G''$). With time elapsed, gel rigidity is further restored *via* healing of the network structure, primarily through relaxations and interpenetration among the fibrils at the boundaries of percolating domains.

This model also can help explain how gel recovery and healing behavior are affected by shear treatment; specifically, why both the initial G' value after thinning, and final, healed gel rigidity, depend on shear duration or shear rate applied to make the gel flow. These dependencies can be explained by the likelihood that certain amounts of small network fragments and/or even smaller fibril fragments break off from gel domains during shear and are no longer network components of the final, restored network. As stated earlier, once flow stops, the network domains immediately percolate with each other, forming a gel network spanning the entire gel. With time, these domains further relax and interpenetrate along domain boundaries, thus further stiffening the gel. If small fragments of network and fibrils have broken off from the large hydrogel domains during shear, then they can simply become trapped within pores of existing gel network structure and no longer contribute to the network structure and resultant stiffness. The population of these fragments seems to grow with increasing shear duration and/or shear rate, therefore leading to lower initial G' and lower ultimate recovered gel rigidity, both observed trends in the rheology data in Fig. 3,4,6 and 7 for both MAX1 and MAX8. The model also explains the impact of pre-shear gel rigidity on post-shear gel recovery. Recovery of hydrogels exhibiting higher pre-shear G' produced gels with both higher initial G' after cessation of flow as well as higher ultimate recovered gel rigidity. This is possibly because stiffer gels have higher cross-link density, as do their descendent gel domains after fracture. Therefore, the network reformed from domains of higher crosslink density should always be more rigid throughout the recovery process.

One can gain further insight into the applicability of the above model to the fibrillar, β-hairpin peptide hydrogels by considering shear phenomena of percolated colloidal systems. As mentioned earlier, colloidal systems composed of percolated colloidal particles can also undergo reversible transitions between the solid gel or glassy state and flowing, solution state upon application of shear. Colloidal systems display rheological phenomena like shear-thinning,[50–52,54] yielding,[58,59,61,104] jamming[62,105] and shear banding.[104,106] Most of these studies combined structural investigation of colloidal gels at rest and under flow with rheological measurements in order to understand how the colloidal gel networks are disassembled and reformed. In some cases, shear causes dynamical structural transitions of colloidal suspensions leading to the hindrance or complete lack of flow properties such as jamming[62,105] or shear thickening.[107] However, most similar to the β-hairpin peptide hydrogels presented herein, the application of shear frequently breaks colloidal gel networks and consequently enables the material to yield, shear-thin and flow.[50–52,58,59,61] For some, but not all, colloid systems this gel-sol transition is reversible once flow is ceased. The aspect of this colloidal gel behavior most similar to the β-hairpin peptide gels is that not all

network junction points are lost during shear-thinning, and colloidal gels can still contain large particle aggregates during flow.[50–52,58,59,61]

We propose that the shear-thinning mechanism through which the β-hairpin peptide hydrogels yield and begin to flow, as described earlier, is similar to the colloidal gel shear-thinning mechanisms mentioned above. Namely, physical crosslinks are disrupted (*i.e.* some peptide fibrils are broken and some peptide fibril entanglements are destroyed) due to applied shear providing for the fracture of the network and material flow. However, the network does not break down into individual fibrils or small bundles/fragments of fibrils that align with the flow direction, as clearly indicated by the lack of alignment up to ~200 nm in the SANS and SAXS results. The gel does fracture into domains, larger than ~200 nm, that can then flow during shear, similar to the flow of disrupted colloidal particles. The fibrils within these domains are still randomly distributed and physically crosslinked in contrast to some shear banding wormlike micellar solutions that display distinct alignment in their shear-thinning regime.[108] In addition, the SANS reveals that the geometry and diameter of fibrils remain unchanged within the domains at various shear rates. An important difference can be seen between the network recovery behavior of the β-hairpin peptide hydrogels and most colloidal gels. Once flow has ceased, the recovery of solid-like behavior of the β-hairpin hydrogel is immediate and much faster than many colloidal gels[52] due to the immediate percolation and packing of the crosslinked peptide fibril domains in space and the lack of any requirement for the gel domains to rearrange or relax over longer time scales in order to percolate again. The colloidal gel literature does inspire future work to attempt to directly image gel domains during flow in order to monitor domain size dependence on variables such as initial gel stiffness and shear rate and duration. These studies are forthcoming.

Live–dead assay of injected cells

We have demonstrated how and proposed the mechanisms by which the β-hairpin peptide hydrogels flow and immediately recover solid gel properties and eventually heal relative to their original, pre-shear state. For future application purposes, it is also essential to know how encapsulated payloads such as macromolecular therapeutics[70] or a desired cell type[9] will be affected by flow or will affect the gel flow property. Previously we have shown that C3H10t1/2 mesenchymal stem cells could be evenly encapsulated within MAX8 β-hairpin hydrogel and shear-thin delivered without obvious effects on the viability of the encapsulated payload.[9] To show the generality of this overall strategy of cell delivery, MG63 cells, a progenitor osteoblast cell line from rat, were homogeneously encapsulated in 0.5 wt% MAX8 hydrogel *ex vivo* and then injected onto a borosilicate confocal chamber *via* an 18½ gauge needle. The homogeneous encapsulation was made possible by the fast gelation kinetics of MAX8 with cell growth culture media which ensured an even distribution of cells when kinetically trapped from suspension.[9] Three hours after injection, a live-dead assay was performed on the shear-thin delivered MG63 cells by staining the living cells green with calcein acetoxymethylester and dead cells red with propidium iodide. The gel-cell construct was examined under the confocal microscope as shown in Fig. 15. The vast majority of the MG63 cells remained alive with minimal cell death. Also the cells were still evenly distributed in three dimensions within the gel scaffold. It can be inferred that after injection, the rapid gel restoration kinetics enables the cells to retain their even distribution within the hydrogel without significant rearrangement or settlement of the cells that would occur if the gel network had broken down into small, fibrillar fragments during shear. Therefore, similar to previous studies,[9] shear-thin delivery by syringe injection had little impact on cell viability and cell distribution, which further suggests that these hydrogels can be excellent candidates for injectable therapeutic delivery vehicles due to their unique shear-thinning and recovery properties. In the near future, studies of these

hydrogels will be expanded to examine gel biocompatibility and whether they can properly function as a scaffold *in vivo*.

Conclusion

In summary, behavior of MAX1 and MAX8 β-hairpin peptide hydrogels during and after flow was studied in order to understand mechanisms of gel shear-thinning and rehealing properties. After shear flow, the hydrogels displayed immediate recovery behavior into a solid after being shear-thinned by rheometer or syringe injection. Gel restoration kinetics was observed to be dependent on shear rate, shear duration and pre-shear gel rigidity. Through scattering measurements, the hydrogel fibril network structure (< 200 nm as probed by SANS, <50 nm as probed by SAXS) was found unchanged from the static gel state at various shear rates investigated. Based on these results, a model was proposed to explain how the gel network fractured into domains during shear-thinning and flow but could immediately percolate back into a solid hydrogel after cessation of shear and subsequently heal to a stiffer hydrogel. Finally, it was demonstrated that the shear-thin delivery process of syringe injection had little impact on cell viability and cell spatial distribution, an indication that these peptidic hydrogels are excellent candidates for injectable therapeutic delivery vehicles.

β-Hairpin hydrogel behavior after shear-thinning through either syringe injection or parallel plate rheometer shearing, was studied. Importantly, the hydrogels behave the same after both types of shear-thinning treatments, thus clarifying that the observed shear-thinning and rehealing after flow is representative of authentic bulk gel properties. The structural characterization performed in capillaries and the rheological characterization performed after capillary injection are of particular practical importance since they enable the observation of hydrogel behavior in a geometry similar to actual potential therapeutic uses involving syringe or catheter injection as well as the direct investigation of the ability of the hydrogels to recover from syringe injection.

Although the model proposed here well explains bulk β-hairpin peptide hydrogel shear-thinning and immediate recovery behavior, several things remain to be solved. For example, it is essential to validate whether the domain size during flow varies with shear treatment and/or original gel rigidity prior to shear flow. Also, the exact cause for fibrillar network aging/healing post-shear needs to be elucidated. Future studies will focus on the above as well as critical assessment of β-hairpin peptide hydrogel *in vivo*. Hopefully, the mechanisms discussed here for β-hairpin peptide solid hydrogel shear-thinning flow and immediate recovery may enlighten researchers to help understand network flow and reformation in other shear-thinning hydrogels.

Supplementary Material

Refer to Web version on PubMed Central for supplementary material.

Acknowledgments

This work was supported by National Institutes of Health (NIH) through grant 5P20RR017716-07 and grant R01 DE016386-01 and the National Institute of Standards and Technology (NIST) through the UD-NIST Center of Neutron Science under grant number DOC #70NANB7H6178. The statements, findings, conclusions, and recommendations are those of the authors and do not necessarily reflect the views of NIH, NIST or the U.S. Department of Commerce. Rheo-SANS experiments were conducted with facilities supported partially by the National Science Foundation under agreement DMR-0454672. Support from the UD Center for Neutron Science is acknowledged and we especially would like to thank Dr Paul Butler, Dr Lionel Porcar, Dr Aaron Eberle and Jeff Krzywon for their help with rheo-SANS experiements. X-Ray scattering experiments were conducted with instruments maintained by the Biophysics Collaborative Access Team (BioCAT) at the Advanced Photon Source

(APS) at Argonne National Laboratories (ANL), USA. Use of the APS at ANL was supported by the U.S. Department of Energy, Office of Science, Office of Basic Energy Sciences, under Contract No. DE-AC02-06CH11357. We thank Dr Liang Guo for his help with SAXS experiments, and Wen-shiue Young for his help with the software, SAXSGUI. And we sincerely appreciate invaluable discussions with and insightful advice from Professor Michael E. Mackay, Professor Norman J. Wagner and Professor Gregory B. McKenna.

References

1. Kretlow JD, Klouda L, Mikos AG. Adv. Drug Delivery Rev. 2007; 59:263–273.
2. Branco MC, Schneider JP. Acta Biomater. 2009; 5:817–831. [PubMed: 19010748]
3. Slaughter BV, Khurshid SS, Fisher OZ, Khademhosseini A, Peppas NA. Adv. Mater. 2009; 21:3307–3329. [PubMed: 20882499]
4. Wang DA, Varghese S, Sharma B, Strehin I, Fermanian S, Gorham J, Fairbrother DH, Cascio B, Elisseeff JH. Nat. Mater. 2007; 6:385–392. [PubMed: 17435762]
5. Holland TA, Bodde EWH, Cuijpers V, Baggett LS, Tabata Y, Mikos AG, Jansen JA. OsCar. 2007; 15:187–197.
6. Hosack LW, Firpo MA, Scott JA, Prestwich GD, Peattie RA. Biomaterials. 2008; 29:2336–2347. [PubMed: 18313745]
7. Tayalia P, Mooney DJ. Adv. Mater. 2009; 21:3269–3285. [PubMed: 20882497]
8. Firth A, Aggeli A, Burke JL, Yang XB, Kirkham J. Nanomedicine. 2006; 1:189–199. [PubMed: 17716108]
9. Haines-Butterick L, Rajagopal K, Branco M, Salick D, Rughani R, Pilarz M, Lamm MS, Pochan DJ, Schneider JP. Proc. Natl. Acad. Sci. U. S. A. 2007; 104:7791–7796. [PubMed: 17470802]
10. Yan C, Pochan DJ. Chem. Soc. Rev. 2010; 39:3528–3540. [PubMed: 20422104]
11. Engler AJ, Sen S, Sweeney HL, Discher DE. Cell. 2006; 126:677–689. [PubMed: 16923388]
12. Solon J, Levental I, Sengupta K, Georges PC, Janmey PA. Biophys. J. 2007; 93:4453–4461. [PubMed: 18045965]
13. Mooney DJ, Vandenburgh H. Cell Stem Cell. 2008; 2:205–213. [PubMed: 18371446]
14. Discher DE, Mooney DJ, Zandstra PW. Science. 2009; 324:1673–1677. [PubMed: 19556500]
15. Janmey PA, McCulloch CA. Annu. Rev. Biomed. Eng. 2007; 9:1–34. [PubMed: 17461730]
16. Pelham RJ, Wang YL. Proc. Natl. Acad. Sci. U. S. A. 1997; 94:13661–13665. [PubMed: 9391082]
17. Stevens MM, George JH. Science. 2005; 310:1135–1138. [PubMed: 16293749]
18. Discher DE, Janmey P, Wang YL. Science. 2005; 310:1139–1143. [PubMed: 16293750]
19. Toledano S, Williams RJ, Jayawarna V, Ulijn RV. J. Am. Chem. Soc. 2006; 128:1070–1071. [PubMed: 16433511]
20. Yang Z, Ma M, Xu B. Soft Matter. 2009; 5:2546–2548.
21. Mosiewicz KA, Johnsson K, Lutolf MP. J. Am. Chem. Soc. 2010; 132:5972–5974. [PubMed: 20373804]
22. Collier JH, Messersmith PB. Bioconjugate Chem. 2003; 14:748–755.
23. Jun HW, Yuwono V, Paramonov SE, Hartgerink JD. Adv. Mater. 2005; 17:2612–2617.
24. Collier JH, Messersmith PB. Adv. Mater. 2004; 16:907–910.
25. Capito RM, Azevedo HS, Velichko YS, Mata A, Stupp SI. Science. 2008; 319:1812–1816. [PubMed: 18369143]
26. Stevens MM, Qanadilo HF, Langer R, Shastri VP. Biomaterials. 2004; 25:887–894. [PubMed: 14609677]
27. Gillette BM, Jensen JA, Tang BX, Yang GJ, Bazargan-Lari A, Zhong M, Sia SK. Nat. Mater. 2008; 7:636–640. [PubMed: 18511938]
28. Aulisa L, Dong H, Hartgerink JD. Biomacromolecules. 2009; 10:2694–2698. [PubMed: 19705838]
29. Yokoi H, Kinoshita T, Zhang SG. Proc. Natl. Acad. Sci. U. S. A. 2005; 102:8414–8419. [PubMed: 15939888]
30. Wang XQ, Kluge JA, Leisk GG, Kaplan DL. Biomaterials. 2008; 29:1054–1064. [PubMed: 18031805]

31. Hacker MC, Klouda L, Ma BB, Kretlow JD, Mikos AG. Biomacromolecules. 2008; 9:1558–1570. [PubMed: 18481893]
32. Wang S, Nagrath D, Chen PC, Berthiaume F, Yarmush ML. Tissue Eng. A. 2008; 14:227–236.
33. Cohn D, Sosnik A, Garty S. Biomacromolecules. 2005; 6:1168–1175. [PubMed: 15877330]
34. Nagapudi K, Brinkman WT, Thomas BS, Park JO, Srinivasarao M, Wright E, Conticello VP, Chaikof EL. Biomaterials. 2005; 26:4695–4706. [PubMed: 15763249]
35. Petka WA, Harden JL, McGrath KP, Wirtz D, Tirrell DA. Science. 1998; 281:389–392. [PubMed: 9665877]
36. Yan H, Nykanen A, Ruokolainen J, Farrar D, Gough JE, Saiani A, Miller AF. Faraday Discuss. 2008; 139:71–84. [PubMed: 19048991]
37. Nair LS, Starnes T, Ko JWK, Laurencin CT. Biomacromolecules. 2007; 8:3779–3785. [PubMed: 17994699]
38. Bhattarai N, Ramay HR, Gunn J, Matsen FA, Zhang MQ. J. Controlled Release. 2005; 103:609–624.
39. Gil ES, Frankowski DJ, Spontak RJ, Hudson SM. Biomacromolecules. 2005; 6:3079–3087. [PubMed: 16283730]
40. Li Q, Wang J, Shahani S, Sun DDN, Sharma B, Elisseeff JH, Leong KW. Biomaterials. 2006; 27:1027–1034. [PubMed: 16125222]
41. Buxton AN, Zhu J, Marchant R, West JL, Yoo JU, Johnstone B. Tissue Eng. 2007; 13:2549–2560. [PubMed: 17655489]
42. Declercq HA, Cornelissen MJ, Gorskiy TL, Schacht EH. J. Mater. Sci.: Mater. Med. 2006; 17:113–122. [PubMed: 16502243]
43. Aimetti AA, Machen AJ, Anseth KS. Biomaterials. 2009; 30:6048–6054. [PubMed: 19674784]
44. Polizzotti BD, Fairbanks BD, Anseth KS. Biomacromolecules. 2008; 9:1084–1087. [PubMed: 18351741]
45. Sharma B, Williams CG, Khan M, Manson P, Elisseeff JH. Plast. Reconstr.Surg. 2007; 119:112–120. [PubMed: 17255664]
46. Shah RN, Shah NA, Lim MMD, Hsieh C, Nuber G, Stupp SI. Proc. Natl. Acad. Sci. U. S. A. 2010; 107:3293–3298. [PubMed: 20133666]
47. Silva GA, Czeisler C, Niece KL, Beniash E, Harrington DA, Kessler JA, Stupp SI. Science. 2004; 303:1352–1355. [PubMed: 14739465]
48. Zaccarelli E. J. Phys.: Condens. Matter. 2007; 19:323101.
49. Solomon MJ, Spicer PT. Soft Matter. 2010; 6:1391–1400.
50. Roberts MT, Mohraz A, Christensen KT, Lewis JA. Langmuir. 2007; 23:8726–8731. [PubMed: 17629305]
51. Rueb CJ, Zukoski CF. J. Rheol. 1997; 41:197–218.
52. Wang Q, Wang LM, Detamore MS, Berkland C. Adv. Mater. 2008; 20:236–239.
53. Lynch JM, Cianci GC, Weeks ER. Phys. Rev. E: Stat., Nonlinear, Soft Matter Phys. 2008; 78:031410.
54. Cipelletti L, Manley S, Ball RC, Weitz DA. Phys. Rev. Lett. 2000; 84:2275–2278. [PubMed: 11017262]
55. Varadan P, Solomon MJ. J. Rheol. 2003; 47:943–968.
56. Hoekstra H, Mewis J, Narayanan T, Vermant J. Langmuir. 2005; 21:11017–11025. [PubMed: 16285766]
57. Hoekstra H, Vermant J, Mewis J. Langmuir. 2003; 19:9134–9141.
58. Smith PA, Petekidis G, Egelhaaf SU, Poon WCK. Phys. Rev. E: Stat., Nonlinear, Soft Matter Phys. 2007; 76:041402.
59. Masschaele K, Fransaer J, Vermant J. J. Rheol. 2009; 53:1437–1460.
60. Laurati M, Petekidis G, Koumakis N, Cardinaux F, Schofield AB, Brader JM, Fuchs M, Egelhaaf SU. J. Chem. Phys. 2009; 130:134907. [PubMed: 19355780]
61. Pham KN, Petekidis G, Vlassopoulos D, Egelhaaf SU, Pusey PN, Poon WCK. Europhys. Lett. 2006; 75:624–630.

62. Rissanou AN, Vlassopoulos D, Bitsanis IA. Phys. Rev. E: Stat., Nonlinear, Soft Matter Phys. 2005; 71:011402.
63. Schneider JP, Pochan DJ, Ozbas B, Rajagopal K, Pakstis L, Kretsinger J. J. Am. Chem. Soc. 2002; 124:15030–15037. [PubMed: 12475347]
64. Pochan DJ, Schneider JP, Kretsinger J, Ozbas B, Rajagopal K, Haines L. J. Am. Chem. Soc. 2003; 125:11802–11803. [PubMed: 14505386]
65. Haines LA, Rajagopal K, Ozbas B, Salick DA, Pochan DJ, Schneider JP. J. Am. Chem. Soc. 2005; 127:17025–17029. [PubMed: 16316249]
66. Rajagopal K, Ozbas B, Pochan DJ, Schneider JP. Eur. Biophys. J. Biophys. Lett. 2006; 35:162–169.
67. Salick DA, Pochan DJ, Schneider JP. Adv. Mater. 2009; 21:4120–4123.
68. Rajagopal K, Lamm MS, Haines-Butterick LA, Pochan DJ, Schneider JP. Biomacromolecules. 2009; 10:2619–2625. [PubMed: 19663418]
69. Rughani RV, Salick DA, Lamm MS, Yucel T, Pochan DJ, Schneider JP. Biomacromolecules. 2009; 10:1295–1304. [PubMed: 19344123]
70. Branco MC, Pochan DJ, Wagner NJ, Schneider JP. Biomaterials. 2009; 30:1339–1347. [PubMed: 19100615]
71. Ozbas B, Kretsinger J, Rajagopal K, Schneider JP, Pochan DJ. Macromolecules. 2004; 37:7331–7337.
72. Hule RA, Nagarkar RP, Altunbas A, Ramay HR, Branco MC, Schneider JP, Pochan DJ. Faraday Discuss. 2008; 139:251–264. [PubMed: 19048999]
73. Kretsinger JK, Haines LA, Ozbas B, Pochan DJ, Schneider JP. Biomaterials. 2005; 26:5177–5186. [PubMed: 15792545]
74. Haines-Butterick LA, Salick DA, Pochan DJ, Schneider JP. Biomaterials. 2008; 29:4164–4169. [PubMed: 18687464]
75. Salick DA, Kretsinger JK, Pochan DJ, Schneider JP. J. Am. Chem. Soc. 2007; 129:14793–14799. [PubMed: 17985907]
76. Ozbas B, Rajagopal K, Schneider JP, Pochan DJ. Phys. Rev. Lett. 2004; 93:268106. [PubMed: 15698028]
77. Yucel T, Micklitsch CM, Schneider JP, Pochan DJ. Macromolecules. 2008; 41:5763–5772. [PubMed: 19169385]
78. Branco MC, Nettesheim F, Pochan DJ, Schneider JP, Wagner NJ. Biomacromolecules. 2009; 10:1374–1380. [PubMed: 19391585]
79. Veerman C, Rajagopal K, Palla CS, Pochan DJ, Schneider JP, Furst EM. Macromolecules. 2006; 39:6608–6614.
80. Nagarkar RP, Hule RA, Pochan DJ, Schneider JP. J. Am. Chem. Soc. 2008; 130:4466–4474. [PubMed: 18335936]
81. Larsen TH, Branco MC, Rajagopal K, Schneider JP, Furst EM. Macromolecules. 2009; 42:8443–8450. [PubMed: 20161466]
82. Hule RA, Nagarkar RP, Hammouda B, Schneider JP, Pochan DJ. Macromolecules. 2009; 42:7137–7145.
83. Kloxin AM, Kasko AM, Salinas CN, Anseth KS. Science. 2009; 324:59–63. [PubMed: 19342581]
84. Foo C, Lee JS, Mulyasasmita W, Parisi-Amon A, Heilshorn SC. Proc. Natl. Acad. Sci.U.S.A. 2009; 106:15418–22072. [PubMed: 19706393]
85. Shen W, Kornfield JA, Tirrell DA. Soft Matter. 2007; 3:99–107.
86. Banwell EF, Abelardo ES, Adams DJ, Birchall MA, Corrigan A, Donald AM, Kirkland M, Serpell LC, Butler MF, Woolfson DN. Nat. Mater. 2009; 8:596–600. [PubMed: 19543314]
87. Ma ML, Kuang Y, Gao Y, Zhang Y, Gao P, Xu B. J. Am. Chem. Soc. 2010; 132:2719–2728. [PubMed: 20131781]
88. Jayawarna V, Richardson SM, Hirst AR, Hodson NW, Saiani A, Gough JE, Ulijn RV. Acta Biomater. 2009; 5:934–943. [PubMed: 19249724]
89. Jeong KJ, Panitch A. Biomacromolecules. 2009; 10:1090–1099. [PubMed: 19301930]

90. Aggeli A, Bell M, Boden N, Keen JN, Knowles PF, McLeish TCB, Pitkeathly M, Radford SE. Nature. 1997; 386:259–262. [PubMed: 9069283]
91. Aggeli A, Bell M, Carrick LM, Fishwick CWG, Harding R, Mawer PJ, Radford SE, Strong AE, Boden N. J. Am. Chem. Soc. 2003; 125:9619–9628. [PubMed: 12904028]
92. Mawer PJ, Waigh TA, Harding R, McLeish TCB, King SM, Bell M, Boden N. Langmuir. 2003; 19:4940–4949.
93. Nagarkar, RP.; Schneider, JP. Nanostructure Design: Methods and Protocols. Gazit, Ehud; Nussinov, R., editors. Vol. vol. 474. Totowa, NJ: Humana Press; 2008. p. 61-77.ch. 5
94. Macosko, CW. Rheology: principles, measurements and applications. New York: Wiley-VCH; 1994.
95. Glinka CJ, Barker JG, Hammouda B, Krueger S, Moyer JJ, Orts WJ. J. Appl. Crystallogr. 1998; 31:430–445.
96. Egres RG, Wagner NJ. J. Rheol. 2005; 49:719–746.
97. Egres RG, Nettesheim F, Wagner NJ. J. Rheol. 2006; 50:685–709.
98. Kline SR. J. Appl. Crystallogr. 2006; 39:895–900.
99. Darby, R. Chemical engineering fluid mechanics. New York: Marcel Dekker; 2001.
100. Hammersley AP. ESRF Internal Report. 1997 **ESRF97HA02T**.
101. Alexander, LE. X-ray Diffraction in Polymer Science. New York: Wiley Interscience; 1969.
102. Egres RG, Wagner NJ. J. Rheol. 2005; 49:719–746.
103. Castelletto V, Hamley IW. Biomacromolecules. 2007; 8:77–83. [PubMed: 17206791]
104. Rogers SA, Vlassopoulos D, Callaghan PT. Phys. Rev. Lett. 2008; 100:128304. [PubMed: 18517918]
105. Prasad V, Trappe V, Dinsmore AD, Segre PN, Cipelletti L, Weitz DA. Faraday Discuss. 2003; 123:1–12. [PubMed: 12638850]
106. Dhont JKG, Lettinga MP, Dogic Z, Lenstra TAJ, Wang H, Rathgeber S, Carletto P, Willner L, Frielinghaus H, Lindner P. Faraday Discuss. 2003; 123:157–172. [PubMed: 12638861]
107. Kalman DP, Wagner NJ. Rheol. Acta. 2009; 48:897–908.
108. Liberatore MW, Nettesheim F, Vasquez PA, Helgeson ME, Wagner NJ, Kaler EW, Cook LP, Porcar L, Hu YT. J. Rheol. 2009; 53:441–458.

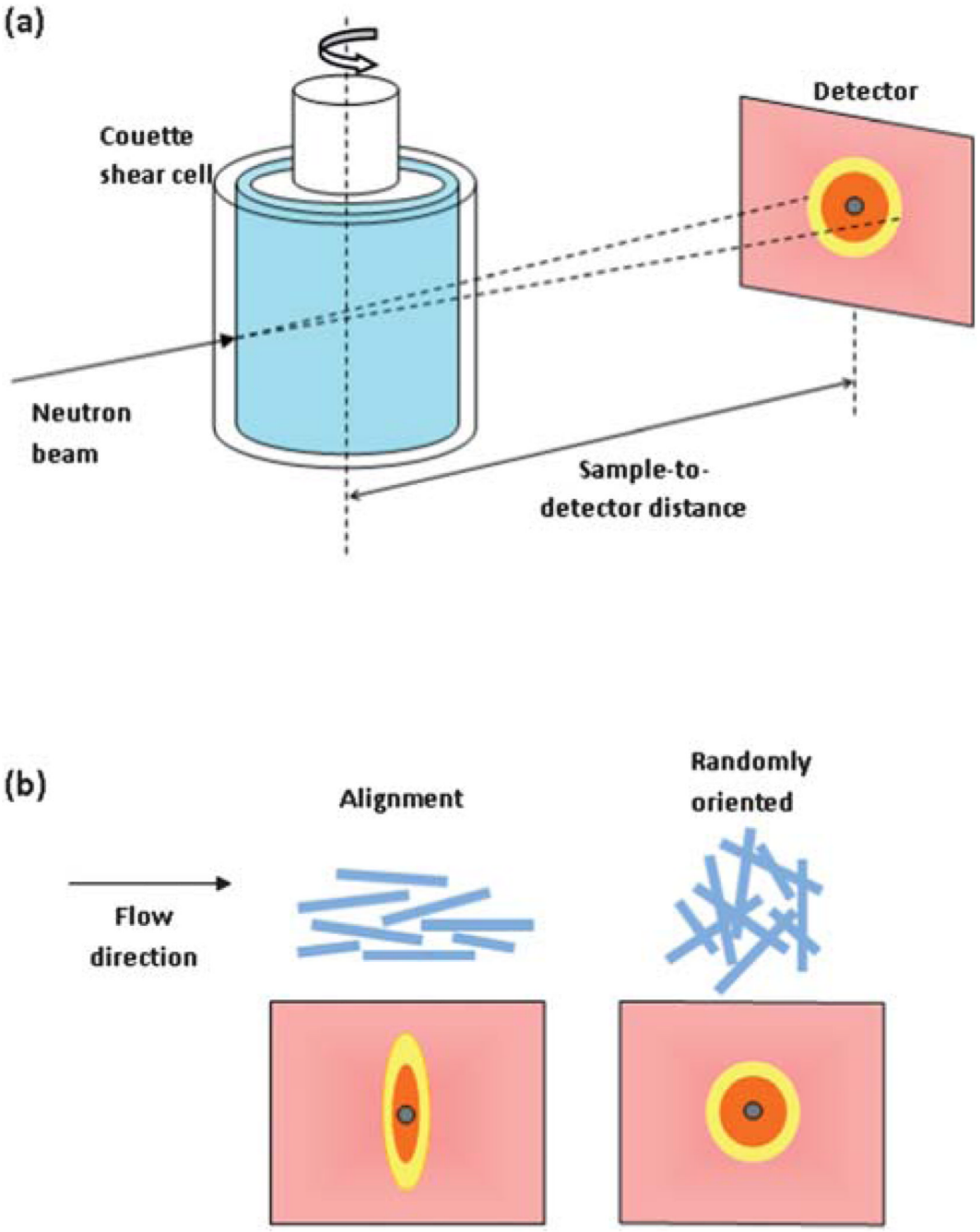

Fig. 1.

(a) Instrumental sketch of rheo-SANS: scattering measurement was performed on fibrillar gel networks subject to steady shear flow in the Couette shear cell. The neutron beam was directed in the radial direction (on-axis). (b) If the fibrils are aligned in the flow direction that points to horizontal right in the rheometer, then the detector will display scattering intensity anisotropy with higher intensity orthogonal to the alignment direction. On the contrary, if the fibrils are randomly oriented under shear flow, the resulting scattering pattern is isotropic as observed when these fibrillar gels are at rest.

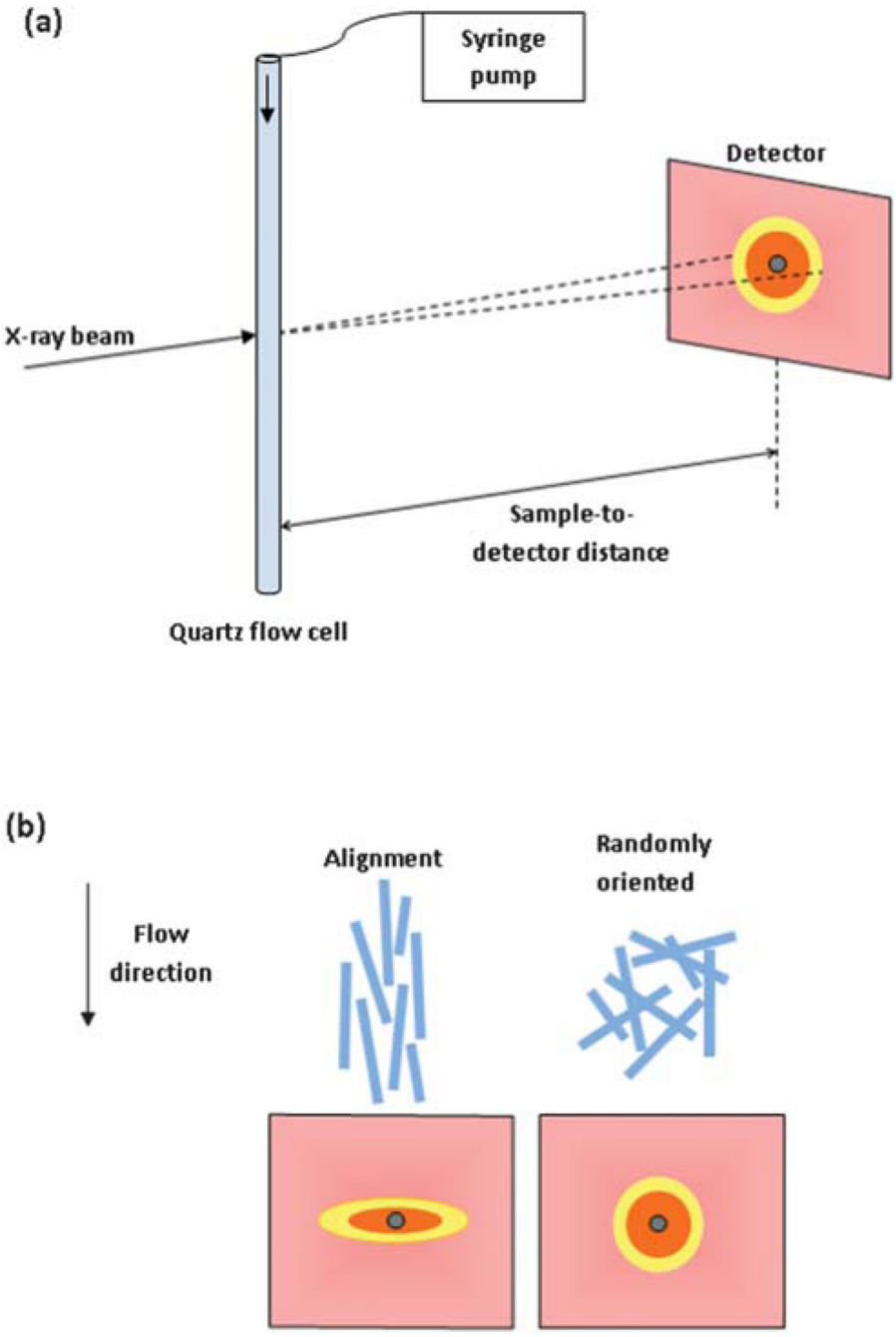

Fig. 2.

(a) Instrumental sketch of small-angle X-ray scattering: scattering measurement was performed on gel when flowing through the quartz capillary flow cell. The X-ray beam was aimed perpendicular through the capillary cross-section. (b) If the fibrils are aligned in the vertical flow direction, the detector will display anisotropic scattering intensity along the horizontal axis. On the contrary, if the fibrils are randomly oriented under capillary flow, the resulting scattering pattern is isotropic just as in the static gel network.

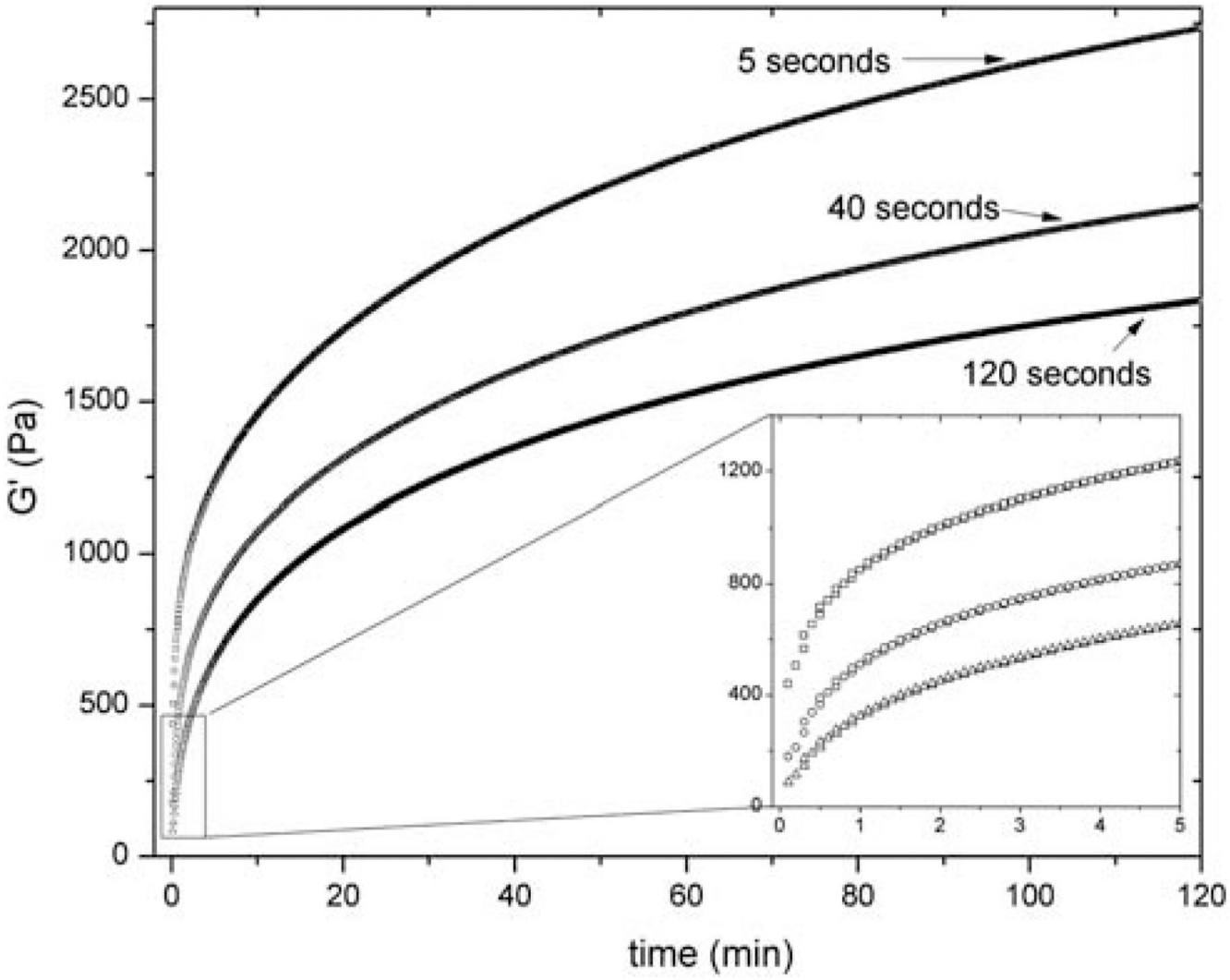

Fig. 3.

Gel restoration kinetics: storage modulus, G′, restored as a function of time after shearing three 2 wt% MAX1 gels formed on the rheometer (pH 7.4, 50 mM BTP, 400 mM NaCl at 20 °C) at a constant shear rate of 1000 s^{-1} for 5 (square), 40 (circle) and 120 s (up triangle), respectively. The inset expands the initial five minutes of gel restoration directly after shear is ceased.

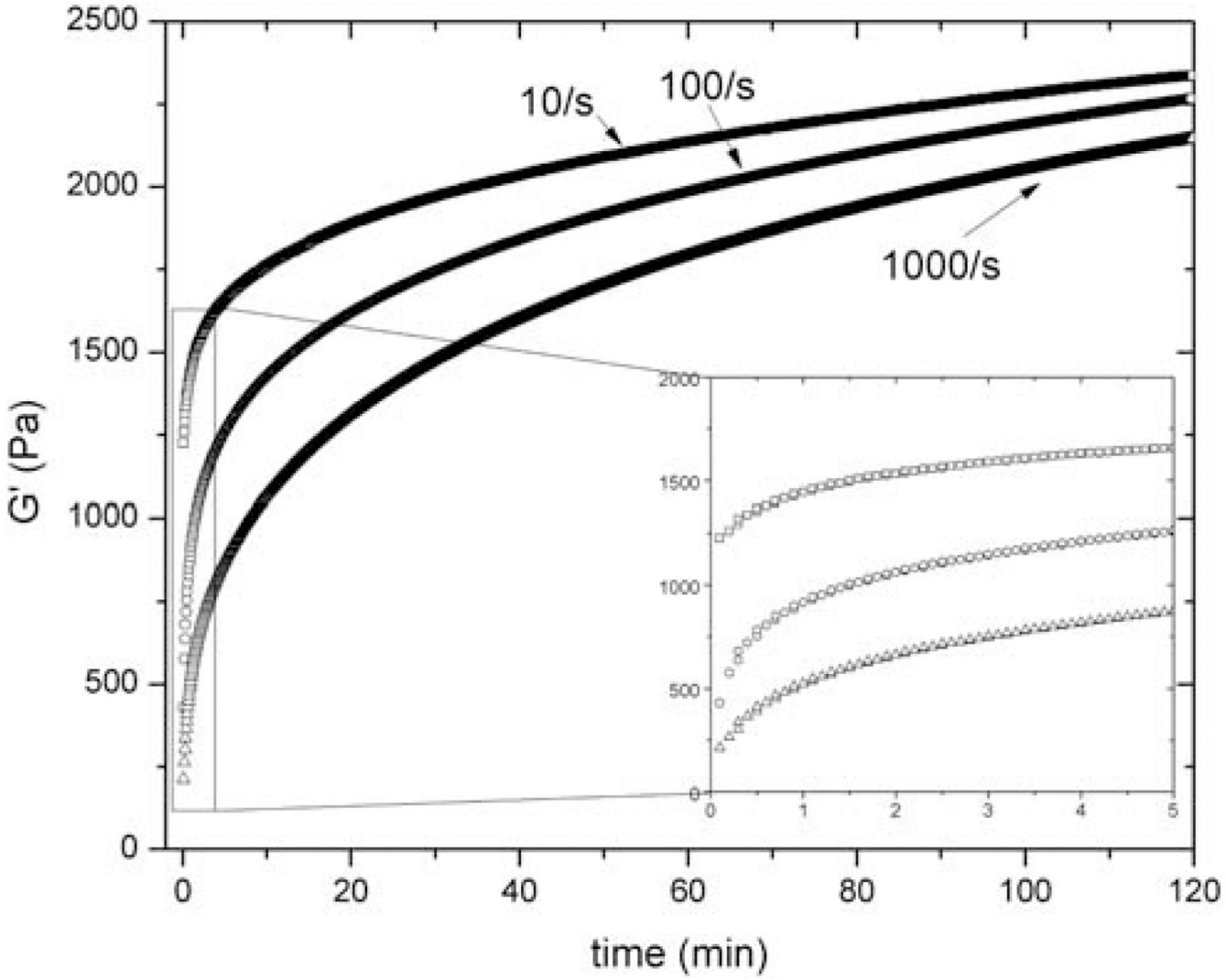

Fig. 4.

Gel restoration kinetics: storage modulus, G′, restored as a function of time after shearing three 2 wt% MAX1 gels (pH 7.4, 50 mM BTP, 400 mM NaCl at 20 °C) formed on the rheometer at a constant shear rate of 10 s^{-1} (square), 100 s^{-1} (circle), 1000 s^{-1} (up triangle) for 40 s, respectively. The inset expands the initial five minutes of gel restoration directly after shear is ceased.

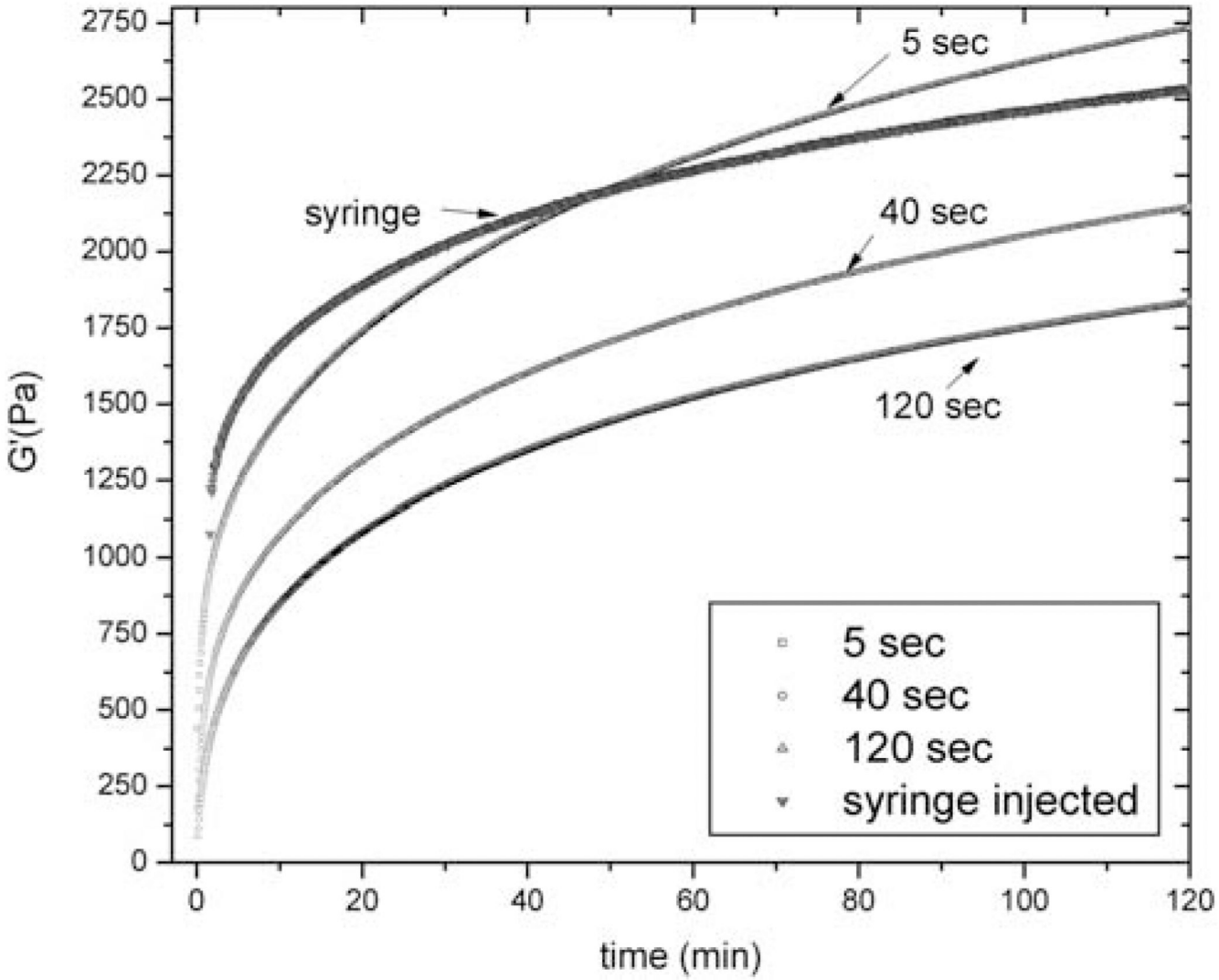

Fig. 5.

Gel restoration kinetics: storage modulus, G′, restored as a function of time after a 2 wt% MAX1 gel (pH 7.4, 50 mM BTP, 400 mM NaCl at 20 °C) was subject to shear induced by syringe injection (grey down triangle) relative to the shear in the rheometer replotted from Fig. 3.

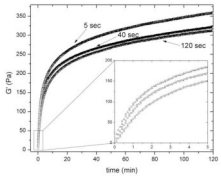

Fig. 6.

Gel restoration kinetics: storage modulus, G′, restored as a function of time after shearing three 0.5 wt% MAX8 gels (pH 7.4, 25 mM HEPES, 37 °C) formed on the rheometer at a constant shear rate of 1000 s^{-1} for 5 s (square), 40 s (circle) and 120 s (up triangle), respectively. The inset zooms in the initial five minutes of gel restoration right after shear is ceased.

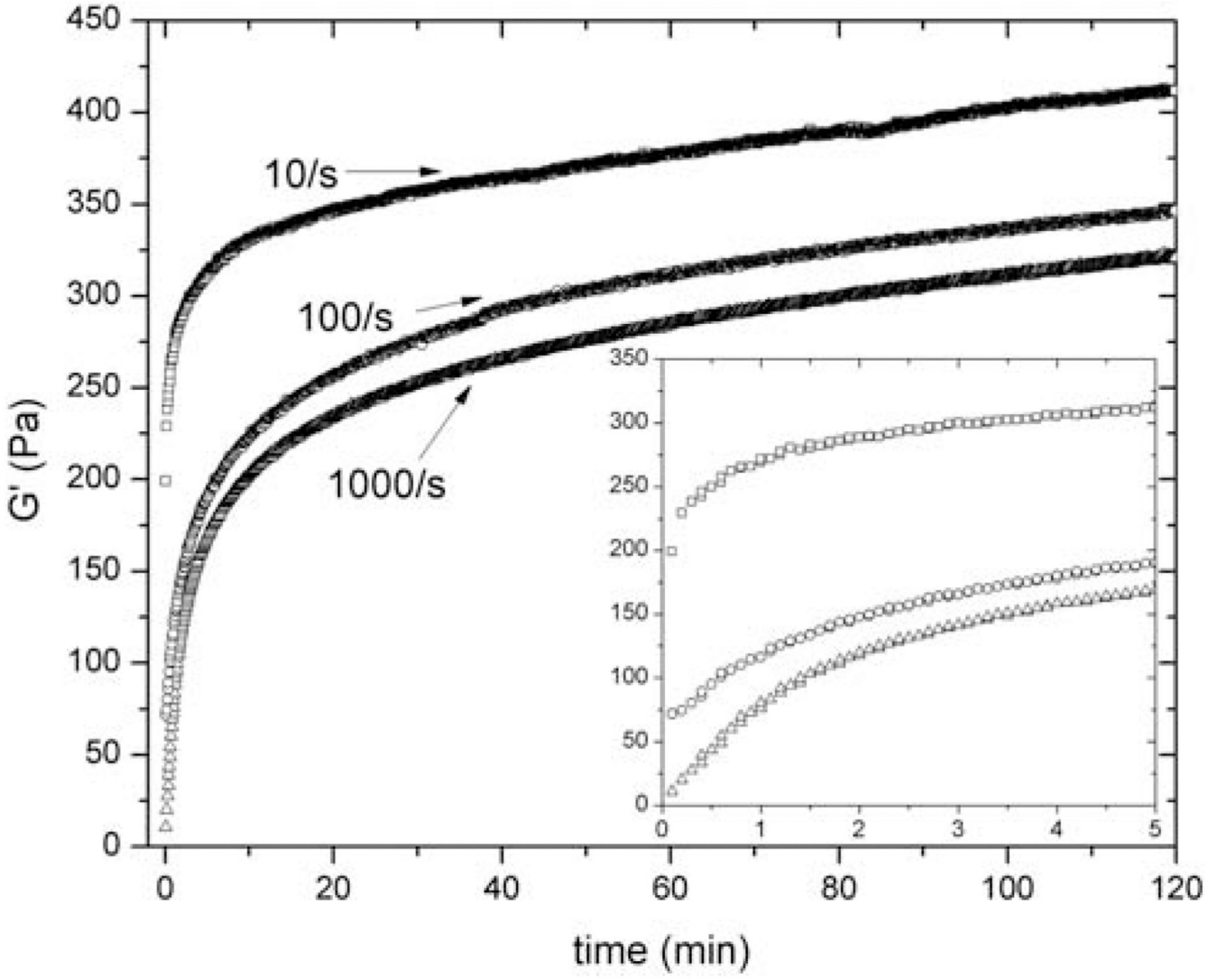

Fig. 7.

Gel restoration kinetics: storage modulus, G′, restored as a function of time after shearing three 0.5 wt% MAX8 gels (pH 7.4, 25 mM HEPES, 37 °C) formed on the rheometer at a constant shear rate of 10 s^{-1} (square), 100 s^{-1} (circle), 1000 s^{-1} (up triangle) for 40 s, respectively. The inset zooms in the initial five minutes of gel restoration right after shear is ceased.

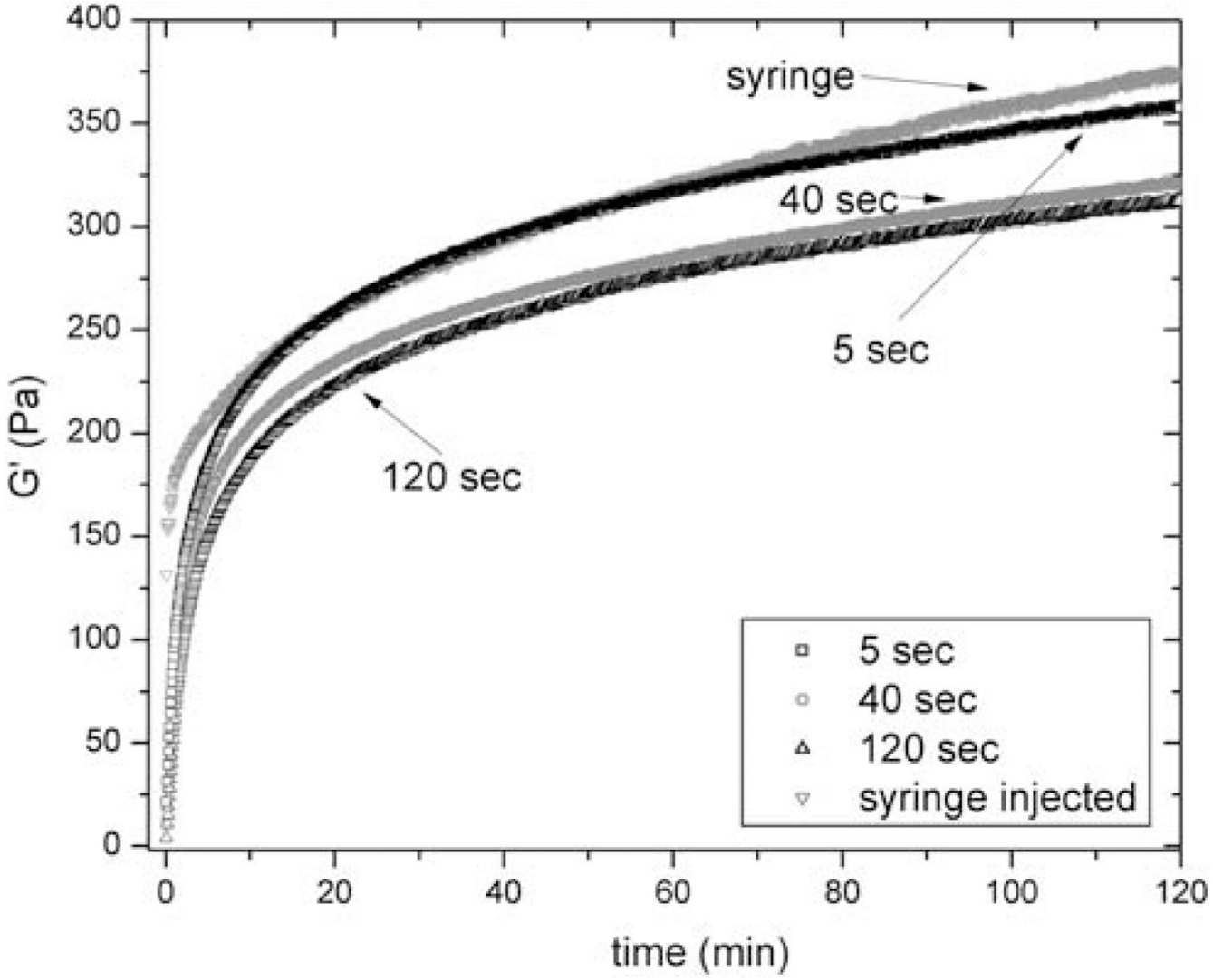

Fig. 8.

Gel restoration kinetics: storage modulus, G′ restored as a function of time after a 0.5 wt% MAX8 gel (pH 7.4, 25 mM HEPES, 37 °C) was subject to shear induced by syringe injection (grey down triangle) relative to the shear in the rheometer replotted from Fig.6.

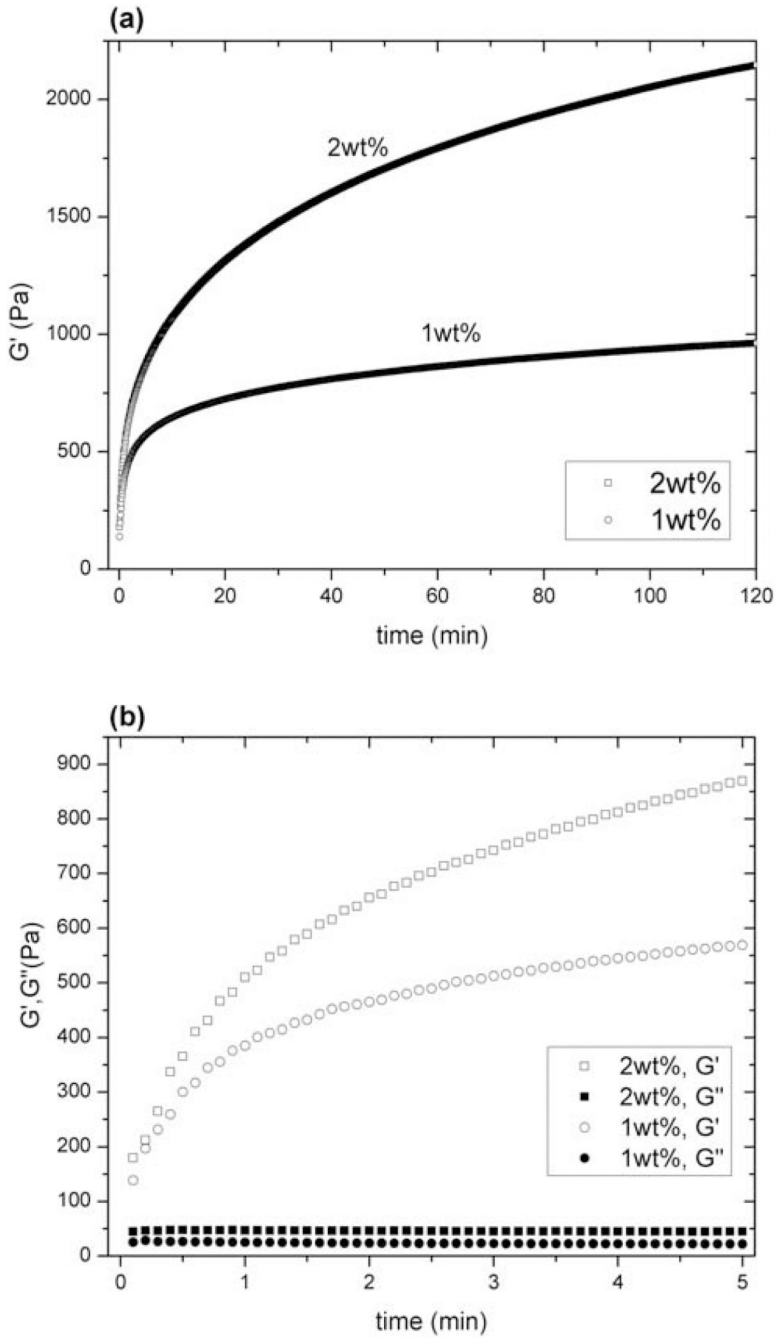

Fig. 9.

Gel restoration kinetics: (a) storage modulus, G′ restored as a function of time after shearing two MAX1 gels (1 and 2 wt% at pH 7.4, 20 °C with 400 mM NaCl) at 1000 s^{-1} for 40 s. (b) Initial five minutes of G′ and G″ restoration right after shear is ceased.

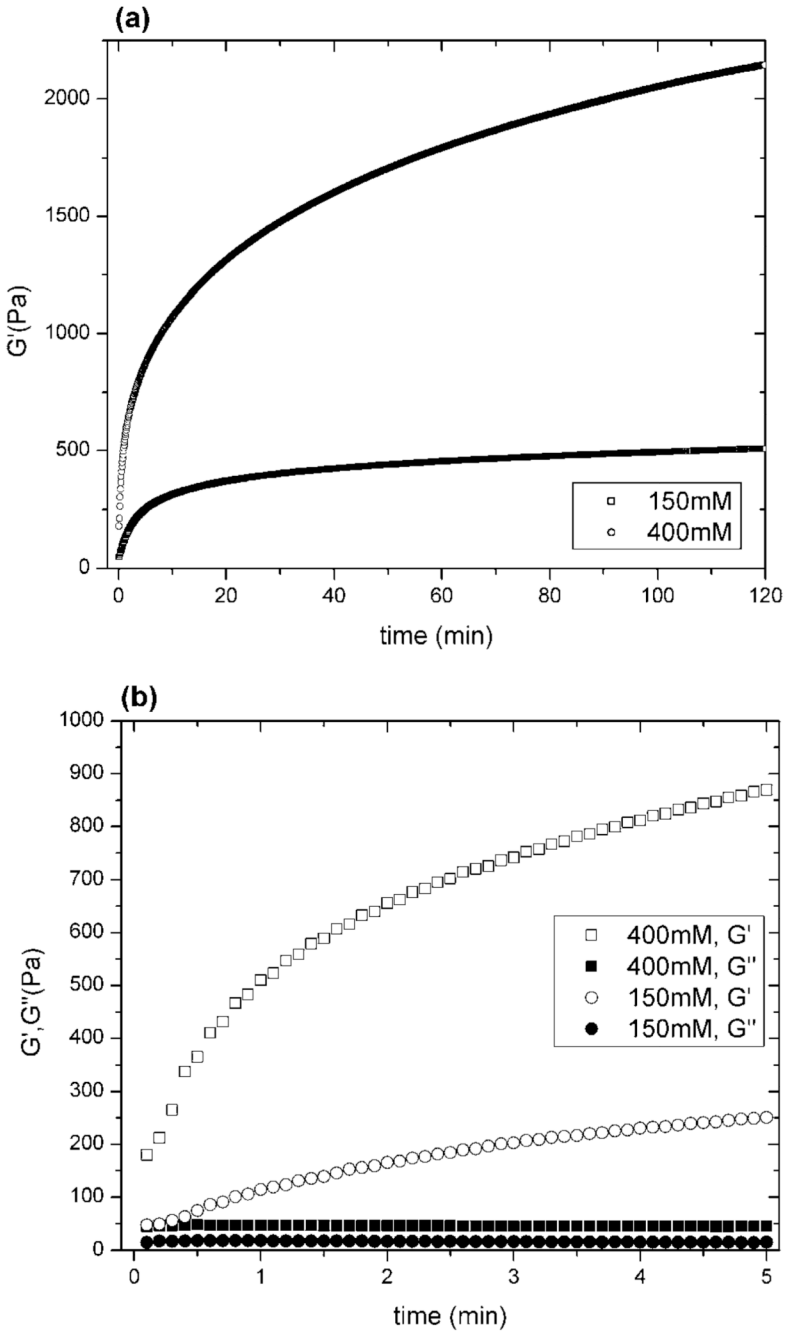

Fig. 10.

Gel restoration kinetics: (a) storage modulus, G′ restored as a function of time after shearing two 2 wt% MAX1 gels (pH 7.4, 20 °C with 150 mM and 400 mM NaCl) at 1000 s^{-1} for 40 s. (b) Initial five minutes of G′ and G″ restoration right after shear is ceased.

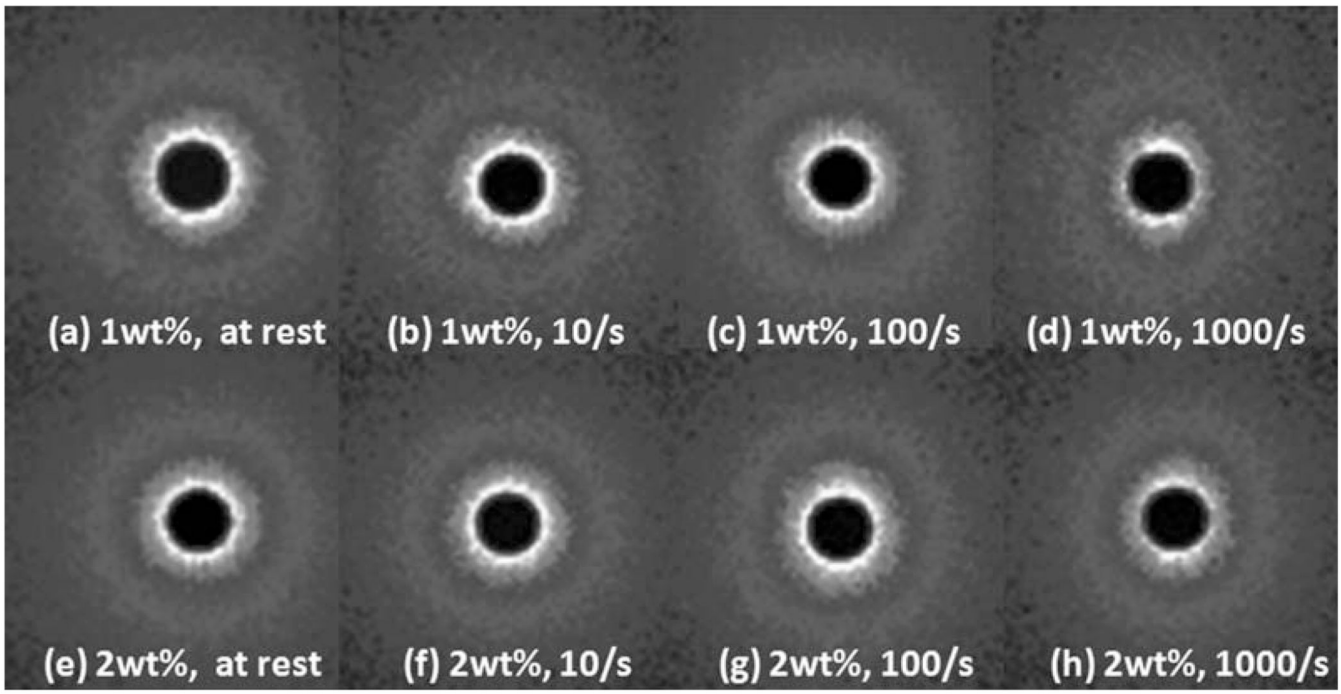

Fig. 11.

Radial 2D scattering patterns obtained from rheo-SANS measurements (0.01 $Å^{-1} < q < 0.3$ $Å^{-1}$) of (a–d) 1 wt% and (e–h) 2 wt% MAX1 (pH 7.4, 400 mM NaCl at 20 °C) gels under shear rate of 0 s^{-1}, 10 s^{-1}, 100 s^{-1} and 1000 s^{-1}. The flow direction points to the horizontal right.

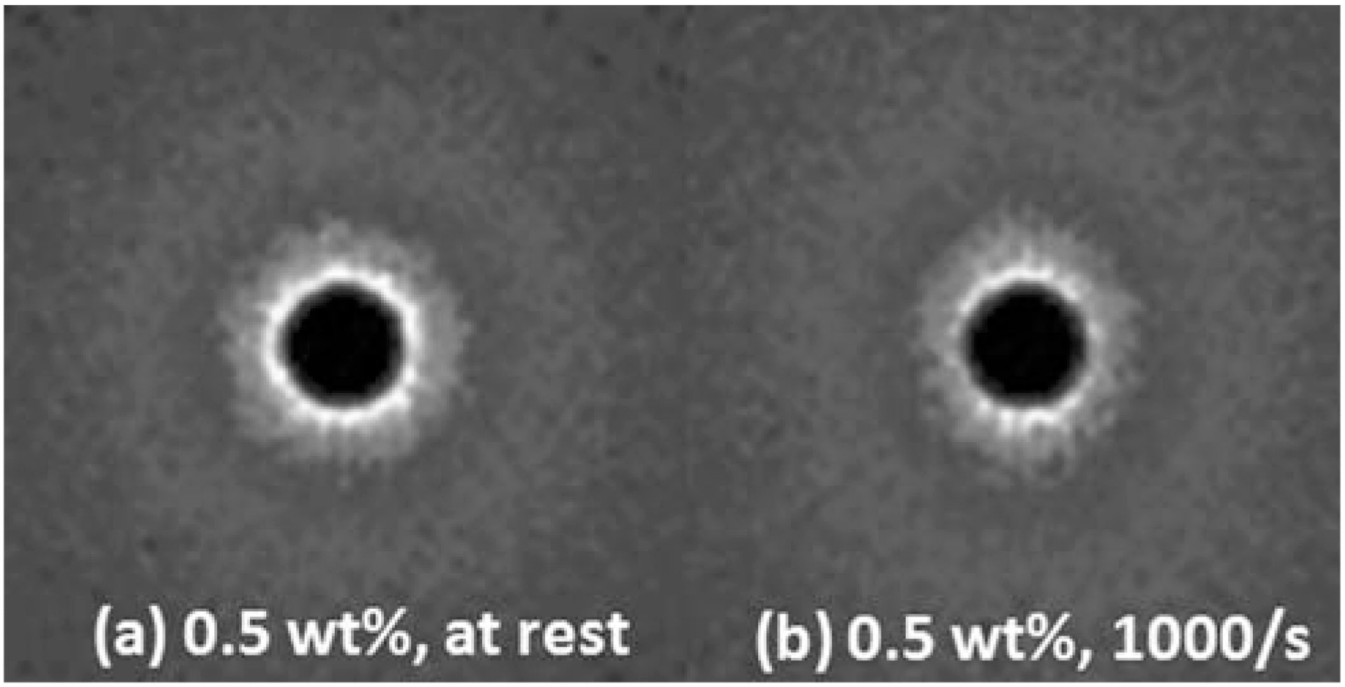

Fig. 12.

Radial 2D scattering patterns obtained from rheo-SANS measurements (0.01 $Å^{-1} < q < 0.3$ A^{-1}) of 0.5 wt% MAX8 (pH 7.4, 37 °C) gels under shear rate of 0 s^{-1} and 1000 s^{-1}. The flow direction points to the horizontal right.

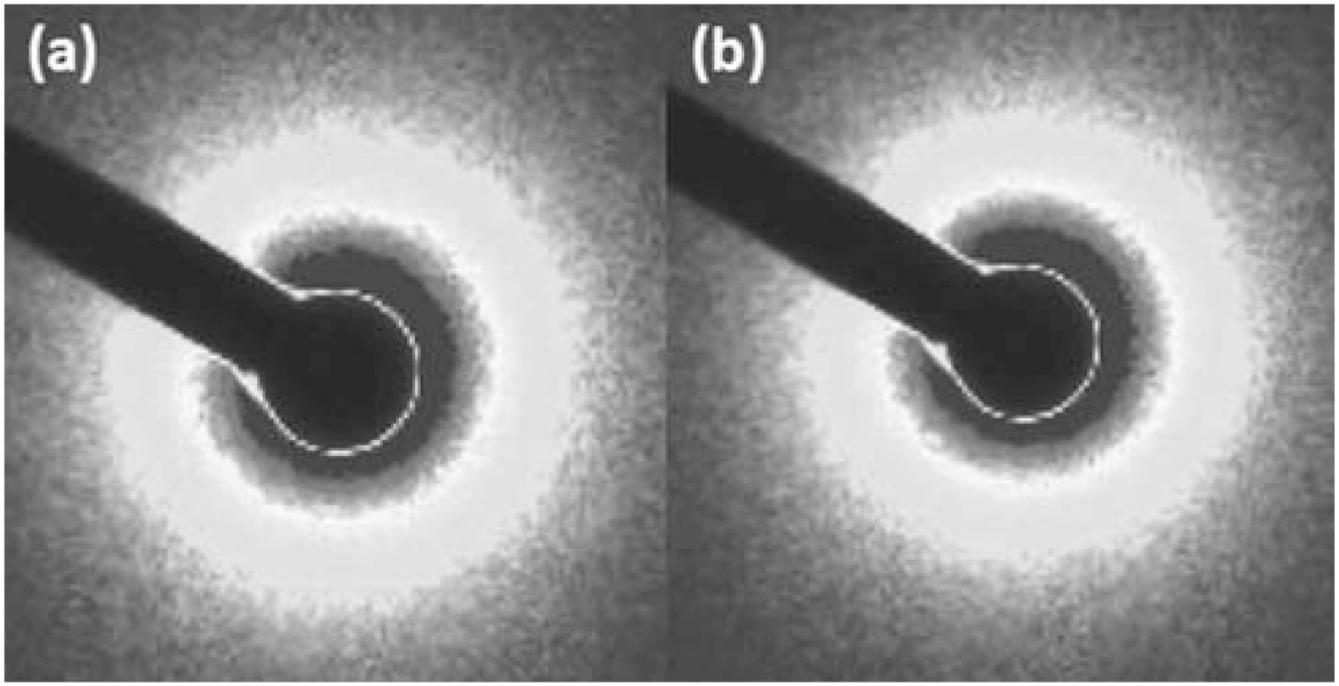

Fig. 13.

2D scattering patterns obtained from SAXS measurements (0.012 $Å^{-1} < q < 0.6\ Å^{-1}$) of 0.5 wt% MAX8 (pH 7.4, 25 mM HEPES, 37 °C) gel (a) at rest and (b) under a constant flow rate of 10 μL min^{-1}. The flow direction points to the horizontal right.

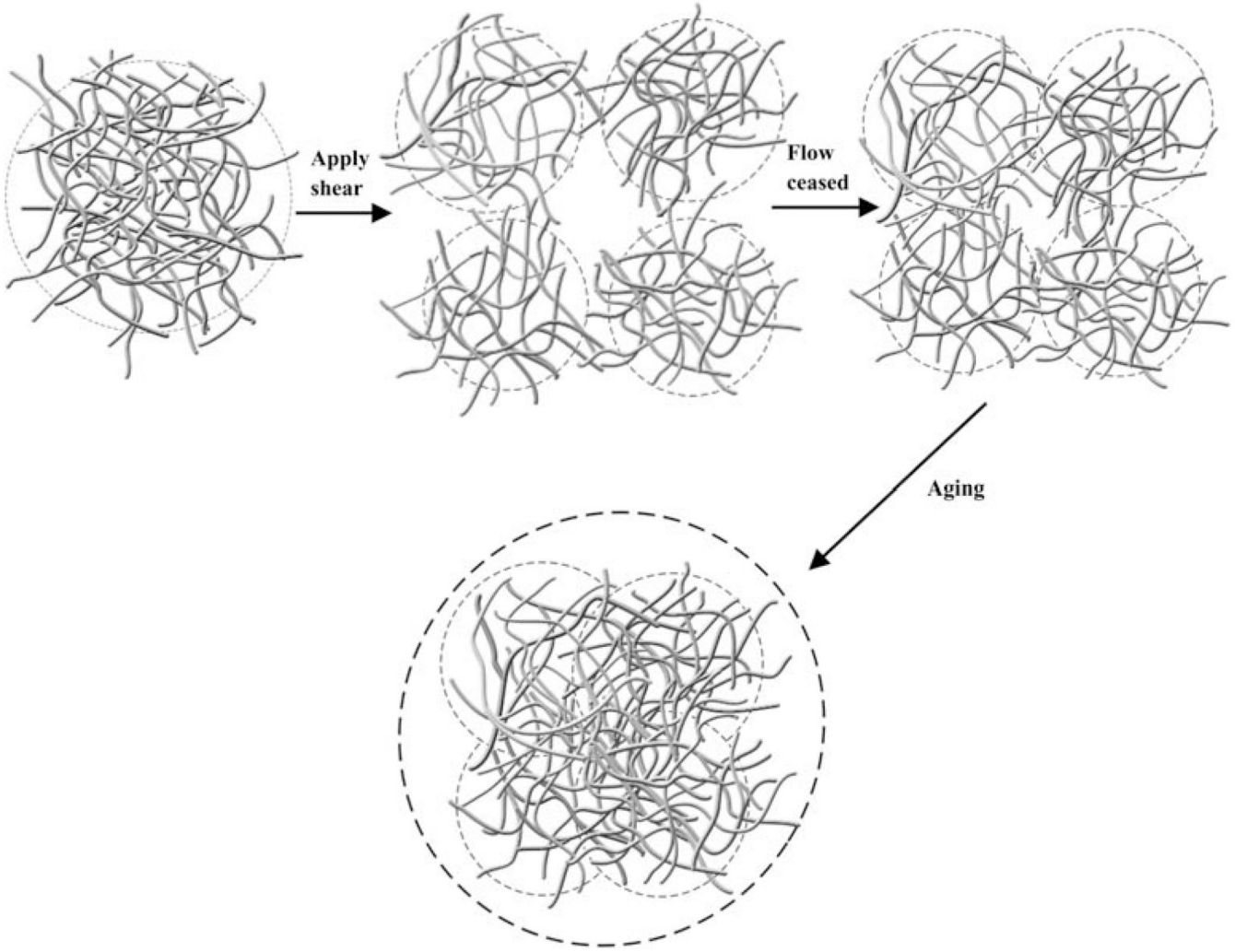

Fig. 14.

Network structure evolution of β-hairpin peptide-based hydrogel during shear-thinning and recovery processes. Under shear, the gel network is fractured into domains that allow the gel to flow. Once the shear has ceased, these domains immediately percolate into a network leading to the immediate recovery of a solid gel response after cessation of shear. Gel rigidity close to values prior to shear is recovered *via* fibrillar network relaxation at the boundaries between previously fractured domains.

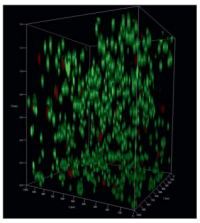

Fig. 15.
Three-dimensional confocal microscope (LSCM) image showing a live–dead assay of MG63 cells encapsulated in 0.5 wt% MAX8 hydrogel. This image was taken three hours after this gel-cell construct was shear-thin delivered *via* an 18-gauge syringe needle. (Red means dead cells and green means living cells).

Table 1

Herman's orientation function, *f*, for 1 wt% and 2 wt% MAX1 hydrogels (pH 7.4, 50 mM BTP, 400 mM NaCl at 20 °C) as well as 0.5 wt% MAX8 hydrogels (pH 7.4, 25 mM HEPES, 37 °C) under various shear rates

	Herman's orientation function		
Shear rate	**1 wt% MAX1**	**2 wt% MAX1**	**0.5 wt% MAX8**
0 s^{-1}	−0.02	−0.02	−0.03
10 s^{-1}	−0.01	−0.05	-
100 s^{-1}	−0.06	−0.04	-
1000 s^{-1}	−0.07	−0.09	−0.09

Table 2

neutron scattering fitting results: fibril radius for 1 wt% and 2 wt% MAX1 hydrogels (pH 7.4, 50 mM BTP, 400 mM NaCl at 20 °C) as well as 0.5 wt% MAX8 hydrogels (pH 7.4, 25 mM HEPES, 37 °C) under various shear rates

	Fibril radius		
Shear rate	**1 wt% MAX1**	**2 wt% MAX1**	**0.5 wt% MAX8**
0 s^{-1}	14.7 Å	16.3 Å	14.7 Å
1000 s^{-1}	13.8 Å	17.4 Å	18.5 Å